EI SEVIER

Contents lists available at ScienceDirect

Acta Biomaterialia

journal homepage: www.elsevier.com/locate/actabiomat



Full length article

In vitro evaluation of MgSr and MgCaSr alloys via direct culture with bone marrow derived mesenchymal stem cells



Wensen Jiang ^a, Aaron F. Cipriano ^{a,b}, Qiaomu Tian ^b, Chaoxing Zhang ^a, Marisa Lopez ^b, Amy Sallee ^b, Alan Lin ^b, Mayra Celene Cortez Alcaraz ^b, Yuanhao Wu ^{c,d}, Yufeng Zheng ^{c,d,*}, Huinan Liu ^{a,b,*}

- ^a Materials Science and Engineering, University of California, Riverside, Riverside, CA 92521, USA
- ^b Department of Bioengineering, University of California, Riverside, Riverside, CA 92521, USA
- ^c Department of Materials Science and Engineering, College of Engineering, Peking University, Beijing 100871, China
- d Center for Biomedical Materials and Tissue Engineering, Academy for Advanced Interdisciplinary Studies, Peking University, Beijing 100871, China

ARTICLE INFO

Article history: Received 20 January 2018 Received in revised form 10 March 2018 Accepted 28 March 2018 Available online 5 April 2018

Keywords:
Biodegradable magnesium alloys
Binary MgSr alloys
Ternary MgCaSr alloys
Bone marrow derived mesenchymal stem
cells (BMSCs)
In vitro direct culture method

ABSTRACT

Magnesium (Mg) and its alloys have been widely investigated as the most promising biodegradable metals to replace conventional non-degradable metals for temporary medical implant applications. New Mg alloys have been developed for medical applications in recent years; and the concept of alloying Mg with less-toxic elements have aroused tremendous interests due to the promise to address the problems associated with rapid degradation of Mg without compromising its cytocompatibility and biocompatibility. Of particular interests for orthopedic/spinal implant applications are the additions of calcium (Ca) and strontium (Sr) into Mg matrix because of their beneficial properties for bone regeneration. In this study, degradation and cytocompatibility of four binary MgSr alloys (Mg-xSr, x = 0.2, 0.5, 1 and 2 wt%) and four ternary MgCaSr alloys (Mg-1Ca-xSr, x = 0.2, 0.5, 1 and 2 wt%) were investigated and compared via direct culture with bone marrow-derived mesenchymal stem cells (BMSCs). The influence of the alloy composition on the degradation rates were studied and compared. Moreover, the cellular responses to the binary MgSr alloys and the ternary MgCaSr alloys were comparatively evaluated; and the critical factors influencing BMSC behaviors were discussed. This study screened the degradability and in vitro cytocompatibility of the binary MgSr alloys and the ternary MgCaSr alloys. Mg-1Sr, Mg-1Ca-0.5Sr and Mg-1Ca-1Sr alloys are recommended for further in vivo studies toward clinical translation due to their best overall performances in terms of degradation and cytocompatibility among all the alloys studied in the present work.

Statement of Significance

Traditional Mg alloys with slower degradation often contain aluminum or rare earth elements as alloying components, which raised safety and regulatory concerns. To circumvent unsafe elements, nutrient elements such as calcium (Ca) and strontium (Sr) were selected to create Mg-Sr binary alloys and Mg-Ca-Sr ternary alloys to improve the safety and biocompatibility of bioresorbable Mg alloys for medical implant applications. In this study, *in vitro* degradation and cellular responses to four binary Mg-xSr alloys and four ternary Mg-1Ca-xSr alloys with increasing Sr content (up to 2 wt%) were evaluated in direct culture with bone marrow derived mesenchymal stem cells (BMSCs). The roles of Sr and Ca in tuning the alloy microstructure, degradation behaviors, and BMSC responses were collectively compared in the BMSC direct culture system for the first time. The most promising alloys were identified and recommended for further *in vivo* studies toward clinical translation.

© 2018 Acta Materialia Inc. Published by Elsevier Ltd. All rights reserved.

E-mail addresses: yfzheng@pku.edu.cn (Y. Zheng), huinan.liu@ucr.edu (H. Liu).

1. Introduction

Magnesium (Mg) shows great potentials for orthopedic device applications as a bioresorbable implant material [1,2]. In the human body, Mg naturally degrades by reacting with water in physiological fluids, which eliminates the necessity of a secondary

^{*} Corresponding authors at: Department of Materials Science and Engineering, College of Engineering, Peking University, No.5 Yi-He-Yuan Road, Hai-Dian District, Beijing 100871, China (Y. Zheng). Department of Bioengineering, Materials Science and Engineering Program, Stem Cell Center, Cell, Molecular and Developmental Biology (CMDB) Program, University of California at Riverside, 900 University Avenue, Riverside, CA 92521, USA (H. Liu).

removal procedure for an implant. The main degradation products of Mg, i.e. magnesium (Mg²⁺) ions, is one of the most abundant ions in the human body, which participates in over 300 enzymatic metabolisms [3,4]. Mg also has a similar elastic modulus to that of human cortical bone [5]. Consequently, Mg-based implants could potentially reduce the stress shielding to fractured bone during healing process [6,7]. Mg-based implants degrade in vivo and are replaced by new bone tissue, which eliminates the need for a secondary revision surgery to remove the implant from human body and significantly decreases further complications and medical cost [8,9]. Unfortunately, the rapid degradation rate of pure Mg in physiological environment may lead to sharp increase of local pH and possible premature mechanical failure of the implants [10], which limited its broad medical applications. Thus, it is critical to improve the corrosion resistance of Mg-based alloys for their potential orthopedic device applications [11]. The compositional design of Mg-based implants, especially the selection of suitable alloying elements of Mg alloys with enhanced corrosion resistance and mechanical properties, is of great importance to the development of biodegradable Mg alloys [12-14]. Different elements and composition may tailor the mechanical and physical properties differently because of the changes in the microstructure and phase distribution [8,15–18]. It is preferred that the metallic ions released from Mg alloys could promote bone tissue healing with minimal adverse effects [15]. However, metallic ions in many cases are not perfectly biocompatible. Admittedly, metallic elements, such as aluminum and yttrium, could result in promising Mg alloys with improved corrosion resistance and/or mechanical strength [19], but these alloying elements were initially designed for nonbiomedical applications and the aluminum and rare earth elements were reported to be potentially harmful to human health [20]. Therefore, recent efforts on the development of new Mg alloys with elements that are naturally present in the human body, such as calcium (Ca) and strontium (Sr), has drawn growing attention [21.22].

Ca is a major component of the human bone, and is essential for a variety of cellular functions [12]. Ca also shows a great grainrefining effect on Mg alloys. The grain size reaches a stable level with the addition of 0.5% Ca, and decreases slightly with any further addition of Ca [23]. The addition of excessive Ca accelerates the corrosion of Mg-Ca alloys, and the optimal concentration of Ca should be < 1.0 wt% [21,23]. Our previous results indicated that the mechanical properties of Mg-Ca alloys could be adjusted by controlling the Ca content and processing treatment [21]. The yield strength (YS), ultimate tensile strength (UTS) and elongation decreased with increasing Ca content [21]. The UTS and elongation of as-cast Mg-1Ca alloy $(71.38 \pm 3.01 \text{ MPa} \text{ and } 1.87 \pm 0.14\%)$ were largely improved after hot rolling (166.7 ± 3.01 MPa and $3 \pm 0.78\%$) and hot extrusion (239.63 ± 7.21 MPa and 10.63 ± 0.64%) [21]. Therefore, we chose to use 1.0 wt% Ca in this study as the optimal concentration in Mg alloys for the most promising corrosion behavior and mechanical properties.

Sr shares similar chemical, biological and metallurgical properties with Mg and Ca as they all belong to the group IIA elements in the periodic table [24]. From the viewpoint of biocompatibility and osteogenic activity, Sr, as a critical trace element in the human body (with 99 wt% of Sr stored in bones) [25], has been reported to improve bone tissue growth and inhibit bone resorption *in vivo* [12,22]. From the perspective of materials science, the addition of Sr can refine the grain size of Mg alloys, enhance the corrosion resistance and improve the mechanical properties of Mg alloys to some extent [12,22]. It is reported that the Sr addition should be 2% or less, which ensures a significantly reduced corrosion rate of the Mg-Sr alloys [22,26]. Interestingly, the as-rolled Mg-2Sr alloy exhibited the best combination of strength and ductility, with values of 213.3 ± 17.2 MPa for UTS and 3.2 ± 0.3% for elongation [22].

Specifically, the YTS and UTS values of the as-rolled Mg-Sr alloys increased with increasing amounts of Sr added up to 2 wt%, whereas YTS and UTS decreased when the amount of Sr further increased [22]. In contrast, elongation of the as-rolled Mg-Sr alloys decreased with increasing Sr content [22]. In this light, we chose the range of Sr content up to 2 wt% in Mg alloy design for the optimal overall performance.

Because of the beneficial properties of Ca and Sr in Mg matrix for bone regeneration, two series of Mg alloys, i.e. binary Mg-strontium (MgSr) alloys and ternary Mg-calcium-strontium (MgCaSr) alloys have been designed and developed for potential orthopedic device applications. The preliminary results with preosteoblast (MC3T3-E1 cell) as a cell model indicated that Mg-Ca-Sr ternary alloys possess superior osteogenic activity than the control, while Mg-1Ca-2.0Sr alloy significantly up-regulated the expressions of the transcription factors of Runt-related transcription factor 2 (RUNX2) and Osterix (OSX). Integrin subunits, as well as alkaline phosphatase (ALP), Bone sialoprotein (BSP), Collagen I (COL I), Osteocalcin (OCN) and Osteopontin (OPN). Li et al. proposed that the MgCaSr alloys stimulated the collagen secretion, extracellular mineralization and osteogenesis-related genes expressions of the MC3T3-E1 cells through ERK1/2 pathway [27]. When compared with the MC3T3-E1 cells, bone marrow derived mesenchymal stem cells (BMSCs) are multipotent and capable of differentiating into bone cells such as osteoblasts that are critical for bone regeneration. Moreover, BMSCs and direct culture method have been previously established for studying cytocompatibility of Mg alloys and cell-alloy interactions directly at the interface [18], and demonstrated the suitability as a model system for rapid screening of Mg alloys in vitro for potential applications in bone implants. Rat primary BMSCs are genetically similar to human BMSCs [28], are more convenient to harvest for immediate culture. The objective of this study was to evaluate and compare the degradation and cytocompatibility of four binary Mg-xSr alloys (Mg-xSr, x = 0.2, 0.5, 1 and 2 wt%) and four ternary Mg-Ca-xSr alloys (Mg-1Ca-xSr, x = 0.2, 0.5, 1 and 2 wt%) in direct culture with bone marrow derived mesenchymal stem cells (BMSCs) for skeletal implant applications.

2. Materials and methods

2.1. Preparation of MgSr alloys, MgCaSr alloys and controls

Binary MgSr alloy, ternary MgCaSr alloys, and the Mg-1Ca alloy control were prepared using a metallurgical process that includes melting, casting, solid solution treatment at 340 °C, and hot extrusion at 320 °C. Specifically for this study, Mg-xSr and Mg-1Ca-xSr alloys (x = 0, 0.2, 0.5, 1, 2 wt%) were prepared and details of metallurgical processing were published previously [22,27]. Briefly, 99.7% pure Mg, 99.8% pure Ca, and 99.9% pure Sr were melted at 670 °C in a high purity graphite crucible with 99.99% pure Argon serving as the protective gas. The temperature was then increased to 720 °C and held for 40 min to ensure homogeneity of the alloy melt. The alloy melts were cast into a 250 °C preheated steel mold. The as-cast ingots of the alloys underwent solid solution treatment at 340 °C for 4 h and quenching in water. The heat-treated ingots were hot extruded at 320 °C with an extrusion speed of 2 mm/ min. Subsequently, the disk sample with a diameter of 12 mm and a height of 2 mm were cut from the extruded rods for this study. Mg-1Ca-0Sr alloy served as a Mg-Ca control which contained no Sr (i.e., Mg-1Ca-0Sr). Pure Mg (99.9% purity, Dongguan Eontec Co., Ltd.) served as a pure Mg control (i.e., Mg-OSr). Additionally, another pure Mg control (99.9% purity, 1.0 mm thick, Alfa Aesar, Catalog No. 40604) was included in this study to compare with previously published work [18,29,30], and designated as Mg- α control. Mg-xSr alloys and Mg-1Ca-xSr alloys (x = 0, 0.2,

0.5, 1, 2 wt%) were abbreviated as xSr and 1Ca-xSr for convenience; and all the sample abbreviations are listed in Fig. 1.

All the Mg-based samples were grinded and polished using SiC paper of 240 grit, 600 grit, 800 grit and 1200 grit sequentially and cleaned in 100% ethanol with sonication (VWR® symphony™ Ultrasonic Cleaner) for 5 min in between. Afterwards, the samples were degreased in acetone for 15 min and then in 100% ethanol for 15 min; both under the same sonication.

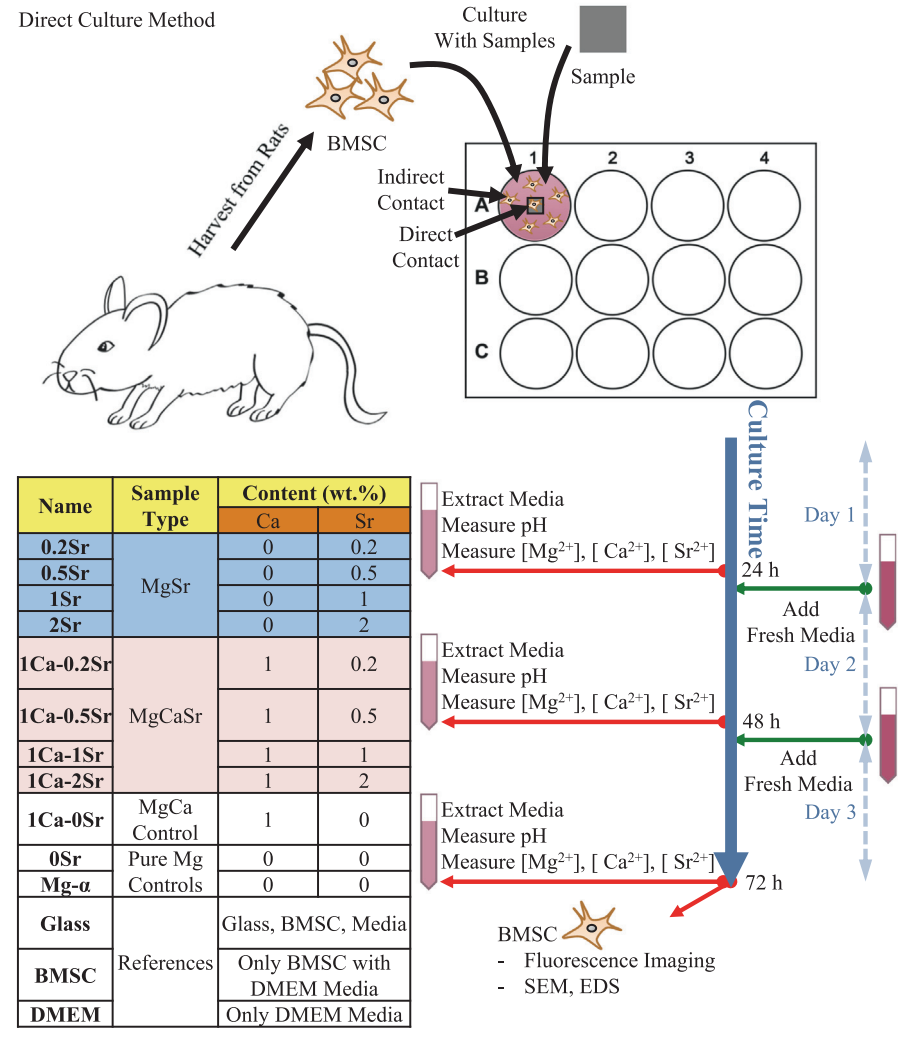
2.2. Measure corrosion resistance of MgSr alloys, MgCaSr alloys and controls using electrochemical method

Corrosion properties of MgSr alloys, MgCaSr alloys and controls were characterized using electrochemical method. Specifically, potentiodynamic polarization (PDP) curves were recorded using a potentiostat/galvanostat (Model 273A, Princeton Applied Research). The PDP testing was performed in a revised stimulated body fluids (rSBF) at 37 °C [18,29–32]. The composition of rSBF was described elsewhere [33]. The samples were cut into 0.2 cm² quarter-circle chips and mounted in epoxy resin (low viscosity castable resin, Pace Technologies Inc). The mounted sample was connected to a working electrode in a three-electrode configuration through the copper wires, and sealed by the epoxy resin.

The epoxy resin completely isolated the copper wires from the rSBF and only one surface of each Mg-based sample was exposed in rSBF. The PDP curves were recorded when the voltage was scanning from 0.5 V to -3.5 V at a scanning rate of 1.2 V/min, and the data was recorded every 0.5 s. Following ASTM G102-89 standard, the corrosion current I_{corr} and the corrosion potential E_{corr} were calculated by extrapolating the tangent line of the anodic and cathodic half of the curves. The corrosion current density J_{corr} was calculated by normalizing I_{corr} with the exposed surface area of each sample.

2.3. Direct culture of Mg alloys with BMSCs

The experimental methods and sample group design for direct culture of Mg alloys and controls with BMSCs in complete Dulbecco's Modified Eagle's medium (DMEM) are illustrated in Fig. 1. Hereafter, DMEM refers to the complete DMEM supplemented with 10% fetal bovine serum (FBS) and 1% penicillin/streptomycin (P/S). In addition to the aforementioned binary MgSr alloys, ternary MgCaSr alloys, Mg-1Ca control and pure Mg controls, the reference groups of glass, BMSC and DMEM were included in this *in vitro* cell culture study. The glass group consisted of glass slides (Fisher Scientific, 1 mm thick, Catalog No.



Sample Group Design for Direct Culture with BMSCs in DMEM

Fig. 1. The illustration of experimental methods and sample group design for in vitro direct culture with BMSCs in DMEM. The samples of interest include binary MgSr alloys, ternary MgCaSr alloys, the controls of MgCa alloy and pure Mg, and the references of glass, BMSC, and DMEM.

12-544-1) that were cut into 5 mm \times 5 mm squares. BMSCs cultured in DMEM without any samples served as the cell-only reference group. The DMEM group without any samples and cells served as the media-only reference. Before cell culture, MgSr alloys, MgCaSr alloys and the controls were disinfected under ultraviolet (UV) radiation for 4 h on all sides. The glass references were degreased and cleaned in acetone and ethanol ultrasonically, and then disinfected under UV radiation for 4 h on all sides.

2.3.1. BMSC culture with MgSr alloys, MgCaSr alloys, controls and references

Following the protocol approved by Institutional Animal Care and Use Committee (IACUC) at the University of California at Riverside (UCR), rat BMSCs were harvested and cultured according to the previously published procedures [18]. BMSCs were cultured to 80-90% confluency in a flask, collected using Trypsin, and seeded directly onto the surface of the disinfected samples at 4 \times 10⁴ cells/cm² at the passage 2 (PN = 2). The seeded BMSCs were incubated in DMEM under standard cell culture conditions (i.e., 37 °C, 95% air, 5% CO₂, sterile, humidified) for 72 h (3 days). The cell culture media were collected and replenished every 24 h, i.e., collected at 24 h, 48 h and 72 h respectively for analyses, replenished with fresh media at 24 h and 48 h respectively. Considering the large numbers of alloy types, the BMSC culture experiments for MgSr alloys and MgCaSr alloys were run separately with their respective controls and references. That is, MgSr alloys, OSr control, Mg- α control and references were grouped together in one culture experiment with one batch of BMSCs; and MgCaSr alloys, 1Ca-0Sr control, and references were grouped together in another culture experiment with another batch of BMSCs.

2.3.2. Post culture media analyses and calculation of in vitro degradation rate

The concentrations of Mg^{2+} , Sr^{2+} and Ca^{2+} ions in the post culture media at 24 h, 48 h and 72 h was measured using inductive coupled plasma optical emission spectrometry (ICP-OES, Optima 8000, Perkin Elmer), as illustrated in the experimental method (Fig. 1). Before ICP-OES, the media of all groups were diluted in deionized (DI) water to minimize the matrix effects. For the measurements of Mg^{2+} and Ca^{2+} ions, the media were diluted at the ratio of 1:100. For the measurement of Sr^{2+} ion, the media were diluted at the ratio of 1:10. The ICP-OES was calibrated using Mg^{2+} , Sr^{2+} and Ca^{2+} standard solutions diluted to the range of 0.5–5.0 mg/L, 0.1–1.0 mg/L and 0.1–1.0 mg/L, respectively.

The degradation rates of Mg alloys were calculated as the daily releasing rate of Mg^{2+} into the culture media. According to the equation of the degradation reaction (Eq. (1) [34]), Mg^{2+} release is an direct indicator of the degradation process.

$$Mg(s) + 2H_2O(l) \rightarrow Mg^{2+} + 2OH^- + H_2(g)$$
 (1)

The daily releasing rates of Mg^{2+} into culture media at day 1 (0 h–24 h), day 2 (24 h–48 h) and day 3 (48 h–72 h) were calculated following Eq. (2). In Eq. (2), R_i represented the daily releasing rates of Mg^{2+} at day 1, day 2 and day 3. C_{Mg} represented Mg^{2+} ion concentration in the culture media measured at the respective 24-h time point, 48-h time point or 72-h time point. $C_{Mg\ in\ DMEM}$ represented the mean Mg^{2+} ion concentration in the DMEM reference measured at the respective 24-h time point, 48-h time point or 72-h time point. V represented the volume of culture media in each culture well (i.e., 3 mL), A represented surface area of the sample, t represented the respective culture time, i.e., t = 1 for 1-day period. $C_{Mg\ in\ DMEM}$ is the baseline of Mg^{2+} ion concentration in the DMEM media for each group, and thus it should be subtracted from the measured total Mg^{2+} ion concentration to obtain the actual amount

of Mg²⁺ ions released from degradation of Mg-based samples. The daily release rate of Mg²⁺ ion into the culture media could be used to directly compare the degradation rate of each alloy type.

$$R_{i=1,2,3} = \frac{\left(C_{Mg} - C_{Mg \text{ in } DMEM}\right)_{i} \times V}{A \times t} \tag{2}$$

The average daily releasing rates of Mg^{2+} into culture media during the entire 3-day culture period was calculated by averaging R_1 , R_2 , and R_3 .

The pH of the post culture media was measured using a precalibrated pH meter (Symphony™, Model SB70P, VWR) immediately after extraction of the media at each daily time point.

2.3.3. Characterize BMSC adhesion and morphology using fluorescence microscopy

After the 3-day culture, BMSCs attached on the samples and plates were fixed with 4% formaldehyde for 30 min. The fixed BMSCs were stained with Alexa Flour® 488-phalloidin (A12379, Life technologies) for F-actin, and 4',6-diamidino-2-phenylindole dilactate (DAPI, Invitrogen) for nuclei. BMSCs attached on each sample (i.e., direct contact) and on the plate around each sample (i.e., indirect contact) were imaged using a fluorescence microscope (Eclipse Ti, Nikon). DAPI-stained nuclei were counted to determine cell adhesion density per unit area. At least five fluorescence images of BMSCs under direct contact condition and nine fluorescence images of BMSCs under indirect contact condition were used for cell counting to ensure the reliability of the results. The adhesion densities of BMSCs under direct or indirect contact conditions were normalized by the mean adhesion density of BMSC reference group from the respective culture. For BMSCs under direct contact conditions, the spreading area per BMSC and the respective aspect ratios were quantified using ImageJ; at least 15 representative BMSCs for each sample, i.e. at least 45 BMSCs for each group, were analyzed. The adhesion density was defined as the number of HUVECs per unit area. The spreading area per HUVEC was defined as the area of F-actin (green color) in the fluorescence image for each HUVEC. The aspect ratio was defined as the ratio of the length of major axis and the length of minor axis for the elliptical fitting of a cell outline.

2.3.4. Characterize cell-material interface using SEM and EDS

The morphologies of BMSCs and elemental distributions at the cell-material interface were characterized using SEM and EDS; and the detailed methods were published previously [18]. Briefly, after 72-h BMSC culture, the samples were moved to a new plate and immersed in 3% glutaraldehyde in phosphate-buffered saline solution for 1 h, which fixed the BMSCs onto the sample surface. The samples were then dehydrated by dip-rinsing in a serial of solutions with increasing ethanol concentration from 50%, 75%, 90% 100%, to 100%, with each rinsing for 10 min. After dehydration, the samples were dried using a critical point dryer (Autosamdri-815, Tousimis Research Corp., Rockville, MD, USA). The samples were sputter coated with Pt/Pd at 20 mA for 40 s to improve the conductivity of their surfaces prior to SEM. The samples were imaged using a scanning electron microscope (SEM, Nova Nano SEM 450, FEI), and the elemental distribution at the cell-material interface was analyzed with energy dispersive X-ray spectroscopy (EDS) using a X-Max50 detector attached to Nova Nano SEM 450. The EDS data were analyzed using AZtecEnergy EDS software (Oxford Instruments, Abingdon, UK).

2.4. Statistical analysis

All numerical data used in this study were obtained from experiments run in triplicate. The numerical data of the corrosion current density, the corrosion potential, the normalized ratio of the

adhesion density of BMSCs under direct contact and under indirect contact conditions were examined using one-way analysis of variance (ANOVA) followed by post-hoc test. The numerical data of ion concentrations in the culture media, the daily releasing rates of $\rm Mg^{2^+}$ ions and the pH in the culture media were examined using two-way analysis of variance (2-way ANOVA) regarding group and culture time as two factors, followed by post-hoc test of different groups with the same culture time. The statistical analysis was performed using GraphPad Prism 7 software. The data were considered statistically significant at p < 0.05.

3. Results

3.1. Corrosion properties of MgSr alloys, MgCaSr alloys and controls

Fig. 2a1 shows the potentiodynamic polarization (PDP) curves of MgSr alloys and controls. All curves have symmetric and smooth profiles, and they were very close to each other. Fig. 2a2 shows the corrosion potential (E_{corr}) and corrosion current density (J_{corr}) of MgSr alloys and controls calculated based on Tafel extrapolation. For the E_{corr} of MgSr alloys, 0.5Sr exhibited a statistically significant less negative E_{corr} than 1Sr. For the comparison between MgSr alloys and controls, Mg- α control showed statistically significant less negative E_{corr} than 0.2Sr, 1Sr and 2Sr. Within the control

groups, no statistically significant difference was detected. For the J_{corr} of MgSr alloys, 1Sr and 2Sr both showed statistically significant lower J_{corr} than 0.2Sr and 0.5Sr. For the comparison between MgSr alloys and controls, all four MgSr alloys showed statistically significant lower J_{corr} than Mg- α . J_{corr} of 0Sr was statistically significant lower than that of 0.5Sr. Among the control groups, 0Sr exhibited statistically significant lower J_{corr} than Mg- α . Overall, 1Sr demonstrated the lowest corrosion rate among MgSr alloys and pure Mg controls of 0Sr and Mg- α .

Fig. 2b1 shows the PDP curves of MgCaSr alloys and controls. All curves have symmetric and smooth profiles, and they were very close to each other. Fig. 2b2 shows the E_{corr} and J_{corr} of MgCaSr alloys and controls calculated based on Tafel extrapolation. For the E_{corr} of MaCaSr alloys, 1Ca-0.2Sr, 1Ca-0.5Sr and 1Ca-1Sr showed statistically significant less negative E_{corr} than 1Ca-2Sr. All other groups showed less negative E_{corr} than 1Ca-2Sr in average, but no statistically significant difference was found. The E_{corr} of MgCaSr alloys showed a trend of increasingly negative E_{corr} with increasing Sr content. For the comparison between MgCaSr alloys and controls, Mg- α control showed statistically significant less negative E_{corr} than 1Ca-1Sr. 1Ca-0Sr control and Mg- α control exhibited statistically significant less negative E_{corr} than 1Ca-2Sr. Within the control groups, no statistically significant difference was detected. For the I_{corr} of MgCaSr alloys, both 1Ca-1Sr and 1Ca-2Sr showed

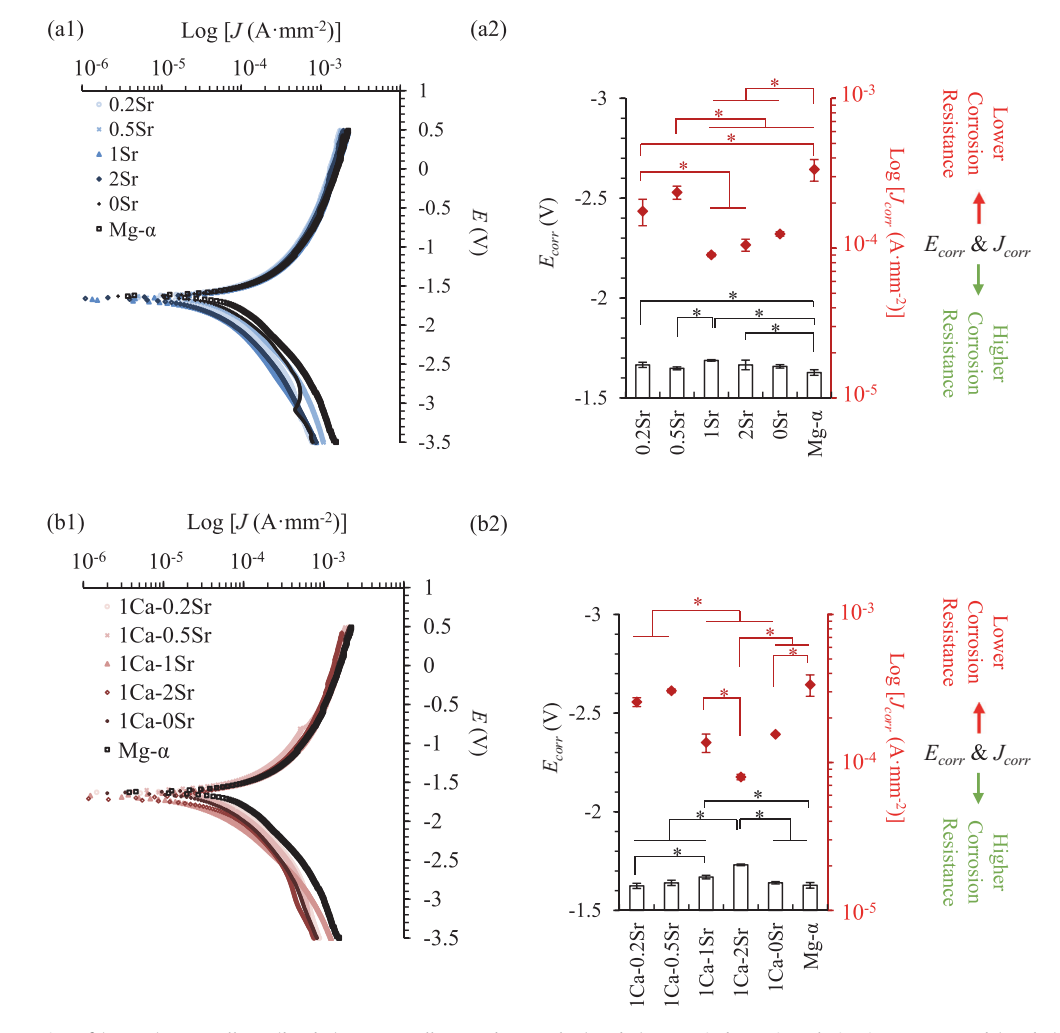


Fig. 2. Corrosion properties of (a1, a2) MgSr alloys, (b1, b2) MgCaSr alloys and controls. (a1, b1) Potentiodynamic polarization curves and (a2, b2) calculated corrosion potential and corrosion current density of (a1, a2) MgSr alloys, (b1, b2) MgCaSr alloys and controls. Hollow bar graphs with their axis on the left show the corrosion potential (E_{corr}); red square symbols with their axis on the right show the corrosion current density (J_{corr}). The corrosion potential and corrosion current density shown in (a2) and (b2) were calculated based on the Tafel extrapolation method. Values are mean \pm standard deviation (n = 3). *p < 0.05. (For interpretation of the references to color in this figure legend, the reader is referred to the web version of this article.)

statistically significant lower J_{corr} than 1Ca-0.2Sr and 1Ca-0.5Sr. 1Ca-2Sr showed statistically significant lower J_{corr} than 1Ca-1Sr. For the comparison between MgCaSr alloys and controls, 1Ca-0Sr control showed statistically significant lower J_{corr} than both 1Ca-0.2Sr and 1Ca-0.5Sr. 1Ca-2Sr exhibited statistically significant lower J_{corr} than 1Ca-0Sr and Mg- α . Within the control groups, 1Ca-0Sr showed statistically significant lower J_{corr} than Mg- α . Overall, 1Ca-2Sr demonstrated the lowest corrosion rate among MgCaSr alloys, MgCa control and Mg- α control.

3.2. Ion concentrations in the post culture media

Fig. 3 shows the Mg²⁺, Sr²⁺, and Ca²⁺ ion concentrations in post culture media and results of statistical analysis. Overall, the results showed that group and culture time are the two factors that significantly affected the concentrations of Mg²⁺, Sr²⁺, and Ca²⁺ ions in the collected media for all groups.

3.2.1. Mg^{2+} ion concentrations in the post culture media

Fig. 3a1 shows Mg²⁺ ion concentrations in the collected media after BMSCs were cultured with MgSr alloys, controls and references at day 1, day 2 and day 3. Culture time was found to be a statistically significant factor that affected the Mg²⁺ ion concentration in the culture media, as summarized in Fig. 3c. Specifically, all MgSr alloys showed a general trend of decreasing Mg²⁺ ion concentration in their culture media with increasing culture time from day 1 and 2 to day 3. Group was another statistically significant factor that affected the Mg²⁺ ion concentration in the culture media, as summarized in Fig. 3c. As expected, all MgSr alloys and pure Mg controls of 0Sr and Mg-α groups showed statistically significant higher Mg²⁺ ion concentrations in their culture media than glass, BMSC and DMEM references at day 1, day 2 and day 3. No statistically significant difference was found among MgSr alloys and pure Mg controls. However, 0.2Sr group showed higher Mg²⁺ ion concentration in the culture media in average than all the other MgSr alloys and pure Mg controls at day 1, day 2 and day 3.

Fig. 3b1 shows the Mg²⁺ ion concentrations in the collected media after BMSCs were cultured with MgCaSr allovs, controls and references at day 1, day 2 and day 3. Culture time was found to be a statistically significant factor that affected the Mg²⁺ ion concentration in the culture media, as summarized in Fig. 3c. Specifically, all MgCaSr alloys showed a general trend of increasing Mg²⁺ ion concentration in their culture media with increasing culture time from day 1 and 2 to day 3, which was opposite trend when compared with the binary MgSr alloys. Group was another statistically significant factor that affected the Mg²⁺ ion concentration in the culture media, as summarized in Fig. 3c. As expected, all MgCaSr alloys, 0Sr and Mg- α controls showed statistically significant higher Mg²⁺ ion concentrations in their respective culture media than glass, BMSC and DMEM references at day 1, day 2 and day 3. No statistically significant difference was found among MgCaSr alloys, 0Sr and Mg- α controls.

3.2.2. Sr^{2+} ion concentrations in the post culture media

Fig. 3a2 shows Sr²⁺ ion concentrations in the collected media after BMSCs were cultured with MgSr alloys, controls and references at day 1, day 2 and day 3. Culture time was found to be a statistically significant factor that affected the Sr²⁺ ion concentration in the culture media, as summarized in Fig. 3c. Specifically, all the MgSr alloys showed decreasing Sr²⁺ ion concentrations in culture media in average from day 1 to day 3. Group was also found to be a statistically significant factor that affected the Sr²⁺ ion concentration in the culture media, as summarized in Fig. 3c. Generally, MgSr alloys with higher Sr content showed greater Sr²⁺ ion concentrations in average in the post-culture media at each time point of day 1, day 2 and day 3; and the four MgSr alloys of 0.2Sr, 0.5Sr, 1Sr,

and 2Sr showed greater Sr²⁺ ion concentrations in average than the pure Mg controls of OSr and Mg-α, and the references of glass, BMSC and DMEM, even though the statistical significance being detected varied at each time point. Specifically, at day 1, pure Mg controls of OSr and Mg- α and all the references showed statistically significant lower Sr²⁺ ion concentrations than 0.5Sr, 1Sr and 2Sr; 0.2Sr showed statistically significant lower Sr²⁺ ion concentrations than 1Sr and 2S; and no statistically significant difference was found between 1Sr and 2Sr. At day 2, pure Mg controls of 0Sr and Mg- α and all the references showed statistically significant lower Sr^{2+} ion concentrations than 1Sr and 2Sr; only Mg- α control and DMEM reference showed statistically significant lower Sr²⁺ ion concentrations than 0.5Sr; and both 0.2Sr and 0.5Sr showed statistically significant lower Sr²⁺ ion concentrations than 2Sr. At day 3, pure Mg controls of OSr and Mg- α and all the references showed statistically significant lower Sr²⁺ ion concentrations than 1Sr and 2Sr; and no statistically significant difference was found among the four MgSr alloys.

Fig. 3b2 shows Sr²⁺ ion concentrations in the collected media after BMSCs were cultured with MgCaSr alloys, controls and references at day 1, day 2 and day 3. Culture time showed statistically significant effect on the Sr²⁺ ion concentrations in the culture media, as summarized in Fig. 3c. Generally, the 1Ca-0.2Sr and 1Ca-0.5Sr showed minimal changes in Sr²⁺ ion concentrations from day 1 to 3; 1Ca-1Sr showed decreasing Sr²⁺ ion concentrations from day 1 to day 3; and 1Ca-2Sr showed decreasing Sr²⁺ ion concentrations from day 1 to day 2 and increasing Sr²⁺ ion concentrations from day 2 to day 3. Group was also found to be a statistically significant factor that affected the Sr²⁺ ion concentration in the culture media, as summarized in Fig. 3c. Generally, the four MgCaSr alloys showed greater Sr²⁺ ion concentrations in average than the pure Mg controls of OSr and Mg-α, and the references of glass, BMSC and DMEM, even though the statistical significance being detected varied at each time point. Specifically, at day 1, all the controls of 1Ca-0Sr and Mg- α and all the references of glass, BMSC and DMEM showed statistically significant lower Sr²⁺ ion concentrations than 1Ca-0.2Sr. 1Ca-1Sr and 1Ca-2Sr: 1Ca-0.2Sr. 1Ca-0.5Sr and 1Ca-1Sr showed statistically significant lower Sr²⁺ ion concentrations than 1Ca-2Sr; and 1Ca-0.5Sr showed statistically significant lower Sr²⁺ ion concentration than 1Ca-1Sr. At day 2, all the controls of 1Ca-0Sr and Mg- α , and all the references of glass, BMSC and DMEM showed statistically significant lower Sr²⁺ ion concentrations than 1Ca-2Sr; 1Ca-0Sr control and DMEM reference both showed statistically significant lower Sr²⁺ ion concentrations than 1Ca-0.2Sr; 1Ca-0.5Sr and 1Ca-1Sr both showed statistically significant lower Sr²⁺ ion concentrations than 1Ca-2Sr; and 1Ca-2Sr showed statistically significant lower Sr²⁺ ion concentrations than 1Ca-0.2Sr. At day 3, all the controls of 1Ca-0Sr and Mg- α , and all the references of glass, BMSC and DMEM showed statistically significant lower Sr²⁺ ion concentrations than 1Ca-0.2Sr and 1Ca-2Sr; 1Ca-0.2Sr, 1Ca-0.5Sr and 1Ca-1Sr all showed statistically significant lower Sr²⁺ ion concentrations than 1Ca-2Sr.

3.2.3. Ca²⁺ ion concentrations in the post culture media

Fig. 3b3 shows the Ca^{2+} ion concentrations in the collected media after BMSCs were cultured with MgCaSr alloys, controls and references at day 1, day 2 and day 3. Culture time was found to be a statistically significant factor that affected the Ca^{2+} ion concentration in the culture media, as summarized in Fig. 3c. Generally, all four MgCaSr alloys, the controls of 1Ca-0Sr and Mg- α , and the glass reference appeared to have a trend of decreasing Ca^{2+} ion concentration in the culture media from day 1 to day 2 and increasing from day 2 to day 3. Group was also a statistically significant factor that affected the Ca^{2+} ion concentration in the culture media, as summarized in Fig. 3c. Specifically, at day 1, all MgCaSr alloys and 1Ca-0Sr control showed statistically significant

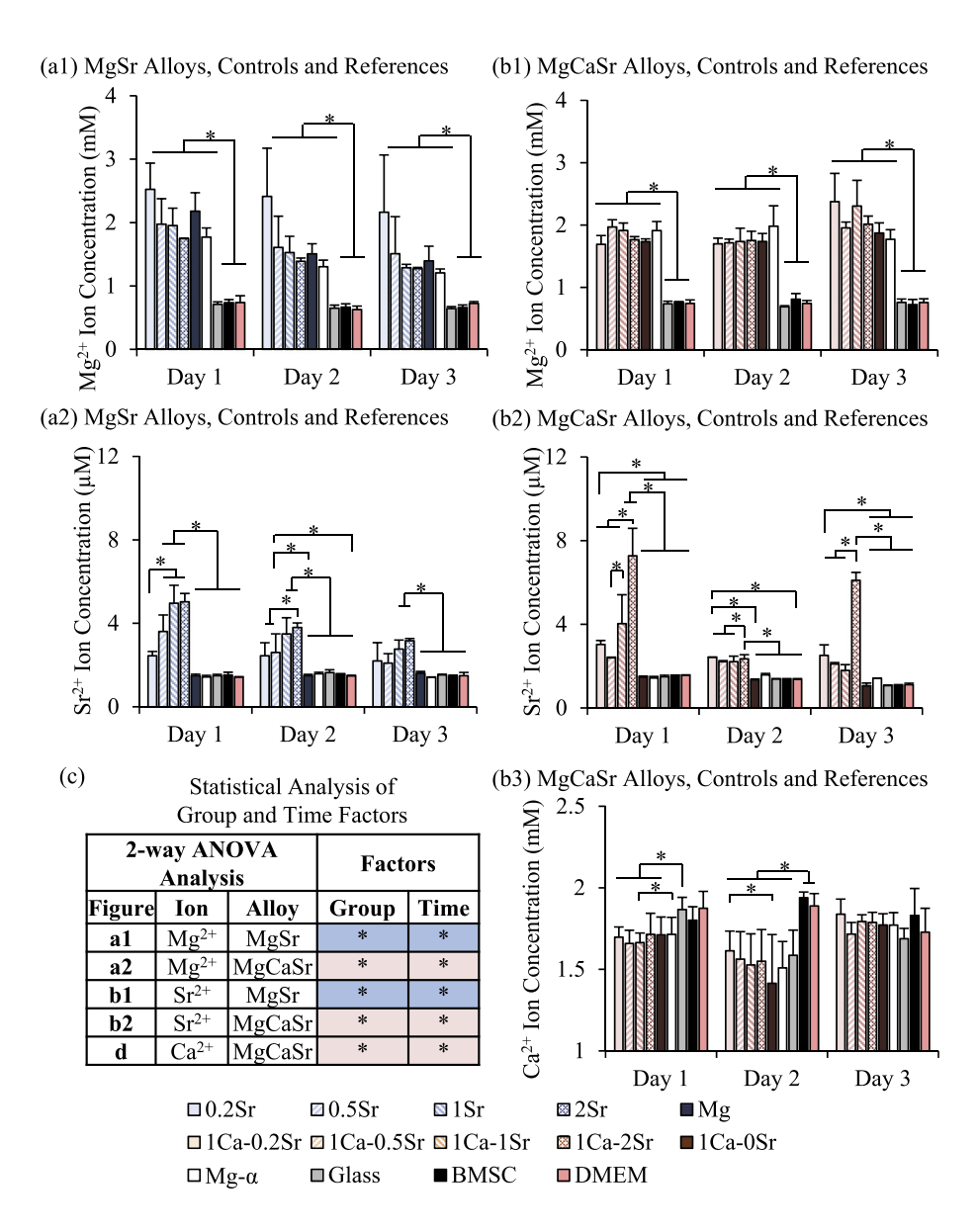


Fig. 3. Ion concentrations in the media after BMSCs were cultured with the (a1, a2) MgSr alloys, (b1, b2, b3) MgCaSr alloys, controls and references. (a1, b1) Mg^{2+} ion concentrations in the media after BMSC culture with (a1) MgSr alloys, controls and references and with (b1) MgCaSr alloys, controls and references. (a2, b2) Sr^{2+} ion concentrations in the media after BMSC culture with (b1) MgSr alloys, references and controls, and with (b2) MgCaSr alloys, references and controls. (b3) Ca^{2+} ion concentrations in the media after BMSC culture with MgCaSr alloys, references and controls. (c) Statistical analysis of the dependency of ion concentrations on group and culture time, analyzed using 2-way ANOVA. Values are mean \pm standard deviation (n = 3). *p < 0.05.

lower Ca^{2+} ion concentrations in the culture media than glass reference; 1Ca-1Sr showed statistically significant lower Ca^{2+} ion concentration in the culture media than $Mg-\alpha$ control; and generally the four MgCaSr alloys and the control groups of 1Ca-0Sr and $Mg-\alpha$ showed lower average Ca^{2+} ion concentration than the references of glass, BMSC and DMEM. At day 2, the four MgCaSr alloys, the controls of 1Ca-0Sr and $Mg-\alpha$, and glass reference showed statistically significant lower Ca^{2+} ion concentrations in their culture media than BMSC and DMEM references; the 1Ca-0Sr control showed statistically significant lower Ca^{2+} ion concentration in the culture media than 1Ca-0.2Sr. At day 3, no statistically significant difference was found among all groups.

3.3. Daily releasing rate of Mg²⁺ in the BMSC/DMEM culture system

Fig. 4 shows the daily releasing rate of Mg²⁺ into the BMSC/DMEM culture with MgSr alloys, MgCaSr alloys and controls at

day 1, 2, and 3, and the average of the entire culture period of 3 days. Culture time was found to be a statistically significant factor that affected the daily releasing rate of Mg²⁺ ions, as summarized in the table in Fig. 4. Specifically, all MgSr alloys and OSr control showed a decreasing daily releasing rates of Mg²⁺ ion from day 1 to day 3. In contrast, for MgCaSr alloys, the groups of 1Ca-0.2Sr and 1Ca-2Sr showed an increasing trend from the day 1 and 2 to day 3 while the values for day 1 and 2 were similar; the groups of 1Ca-0.5Sr and 1Ca-1Sr showed a decreasing trend from day 1 to day 2 and then an increasing trend from day 2 to day 3. Group was also found to be a statistically significant factor that affected the daily releasing rate of Mg²⁺ ions into the BMSC/DMEM culture, as summarized in the table in Fig. 4. Specifically, at day 1, 2Sr showed a statistically significant lower daily releasing rate of Mg²⁺ than 0.2Sr. At day 2, MgSr groups of 0.5Sr, 1Sr, 2Sr, MgCaSr groups of 1Ca-0.5Sr and 1Ca-1Sr, and 0Sr control, showed statistically significant lower rates than 0.2Sr group; 1Ca-0.2Sr, 1Ca-2Sr,

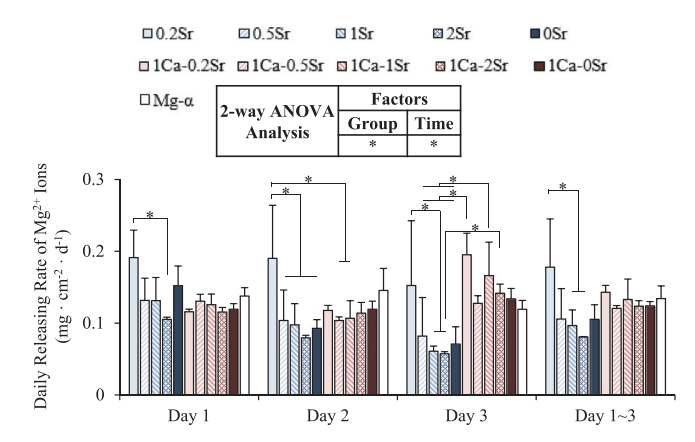


Fig. 4. The daily releasing rates of Mg^{2+} ions into the media of BMSC culture with the MgSr alloys, MgCaSr alloys, controls and references during day 1, day 2, day 3 and the average of entire 3-day culture period (day1-3). The table showed the 2-way ANOVA analysis of dependency of the release rate of Mg^{2+} ions during each day on group and time. Values are mean \pm standard deviation (n = 3). *p < 0.05.

1Ca-0Sr control and Mg- α control also showed lower rates in average than 0.2Sr, but no statistically significant difference was detected. At day 3, the groups of 1Sr and 2Sr showed statistically significant lower rates than 0.2Sr; the groups of 0.5Sr and 0Sr also showed lower rates than 0.2Sr in average, but no statistically significant difference was detected; the group of 0.5Sr, 1Sr, 2Sr and 0Sr showed statistically significant lower rates than 1Ca-0.2Sr and 1Ca-1Sr; and 2Sr showed a statistically significant lower rate than 1Ca-2Sr.

Fig. 4 also showed that, during the entire 3-day culture period, the MgSr groups of 1Sr and 2Sr showed statistically significant lower releasing rates of Mg²⁺ ions than 0.2Sr, and they also showed the lowest average releasing rates of Mg²⁺ ions among all the groups tested. Except for 0.2Sr, all MgSr alloys and 0Sr control showed lower releasing rates in average than the four MgCaSr alloys, 1Ca-0Sr control and Mg- α control. Among the four MgSr alloys, the trend showed that the releasing rates of Mg²⁺ ions decreased with increasing Sr content from 0.2 wt% to 2 wt%. Among the four MgCaSr alloys, the trend was not clear, and 1Ca-0.5Sr and 1Ca-2Sr showed lower releasing rates than 1Ca-0.2Sr and 1Ca-1Sr in average. Interestingly, the Ca addition appeared to neutralize the effects of Sr addition on the releasing rates during the 3-day culture. The effects of Sr content on the Mg²⁺ releasing rates was less pronounced for Mg-1Ca-xSr alloys than for binary Mg-xSr alloys.

3.4. The pH change in the post culture media

Fig. 5 shows the pH change in the collected media after BMSCs were cultured with MgSr alloys, MgCaSr alloys, controls and references at day 1, day 2 and day 3. Both the absolute value of pH in the collected media and the change in pH were plotted in Fig. 5. The statistical significance is summarized in the table at the bottom of Fig. 5. Specifically, the change in pH was defined as the pH increase in each group normalized by the mean pH increase in DMEM reference. That is, the change of pH = Δ pH/ Δ pH_{DMEM}, where the ΔpH was defined as $\Delta pH = pH(t) - pH(start)$ for each group, and the ΔpH_{DMEM} was defined as $\Delta pH_{DMEM} = pH_{DMEM}$ $(t)_{\text{mean}}$ – pH (start). The t represents each prescribed time point (day 1, day 2 and day 3), $pH_{DMEM}(t)_{mean}$ represents the mean pH of DMEM group at time point t. The starting pH for all groups is 7.40, thus pH (start) = 7.40. The change in pH is a mathematical indicator for the tendency of each group to become more alkaline (>1) or more acidic (<1) in comparison with the DMEM reference during the prescribed culture period.

Fig. 5a shows the pH and the change of pH in the media after BMSCs were cultured with MgSr alloys, controls and references. Culture time was found to be a statistically significant factor that affected the pH in the BMSC culture with MgSr alloys, controls and references. Generally, all the MgSr alloys and pure Mg controls of OSr and Mg- α showed more alkaline pH in day 1 and 2 than day 3. Group was another statistically significant factor that affected the pH in the media of BMSCs cultured with MgSr alloys, controls and references. All MgSr alloys showed more alkaline pH than the DMEM reference at day 1 and day 2; at day 3, all the MgSr alloys except for 0.2Sr, showed less alkaline pH than DMEM reference. Statistically, at day 1, 0.2Sr group showed a significant higher pH in the culture media than 1Sr, 2Sr, Mg-α control, glass and BMSC references. At day 2, 0.2Sr and 1Sr groups showed statistically higher pH than DMEM reference: and 0.2Sr, 0.5Sr and 1Sr groups showed statistically higher pH than BMSC reference. At day 3, no statistical significance was found among all four MgSr groups, pure Mg controls and references.

Fig. 5b shows the pH and the change of pH in the media after BMSCs were cultured with MgCaSr alloys, controls and references. Culture time was found to be a statistically significant factor that affected the pH in the media after BMSCs were cultured with MgCaSr alloys, controls and references. Generally, the four MgCaSr alloy groups showed higher pH at day 3 than day 1 and 2, and higher pH than DMEM reference. Group was not a statistically significant factor that affected the media pH in the groups of MgCaSr alloys, controls and references. That is, no statistically significant difference in pH was found among the four MgCaSr alloys, the controls, and references.

3.5. BSMC adhesion and morphology in direct contact and indirect contact

Fig. 6 shows the representative fluorescence images and the quantitative analysis of BMSCs in the direct contact condition (i.e., cells directly attached on the surface of each sample). In the fluorescence images of MgSr alloys (Fig. 6a1-6a4), 0.2Sr and 0.5Sr groups showed that BMSCs sparsely attached on the sample surface, while 1Sr and 2Sr showed visually more BMSCs attached on their surfaces. In the fluorescence images of MgCaSr alloys (Fig. 6b1-6b4), 1Ca-0.5Sr, 1Ca-1Sr and 1Ca-2Sr all showed visually more BMSCs attached on their surfaces than 1Ca-0.2Sr. Fig. 6f shows the cell adhesion density directly on the surface of respective substrates normalized by the cell adhesion density in the BMSC reference group, namely cell density ratio. No statistically significant difference in the cell density ratio was found among all the MgSr alloys, MgCaSr alloys, pure Mg controls of OSr and Mg-α, and 1Ca-OSr control, but 1Ca-0.5Sr, 1Ca-1Sr, 1Ca-2Sr and Mg- α control showed higher cell density ratio in average than all four MgSr alloys, 1Ca-0.2Sr, controls of 0Sr and 1Ca-OSr. Statistically, 0.2Sr, 0.5Sr, 2Sr, OSr control and 1Ca-0.2Sr showed significantly lower cell density ratio than the glass reference.

Fig. 6g shows the spreading area per BMSC in the direct contact conditions when cultured with respective group of samples. The groups of 1Ca-0.2Sr, 1Ca-0.5Sr and 1Ca-2Sr presented statistically larger area per BMSC than 2Sr and Mg- α control. The groups of 0.2Sr, 0.5Sr, glass control and BMSC reference showed statistically larger area per BMSC than Mg- α control. Fig. 6h shows the aspect ratio of BMSCs in the direct contact condition. 1Ca-0.2Sr shows a statistically higher aspect ratio than all the other groups except for Mg- α control. Mg- α control shows a higher aspect ratio than glass control.

Fig. S1 (in supplemental materials) shows the representative fluorescence images and the cell density ratio in the indirect

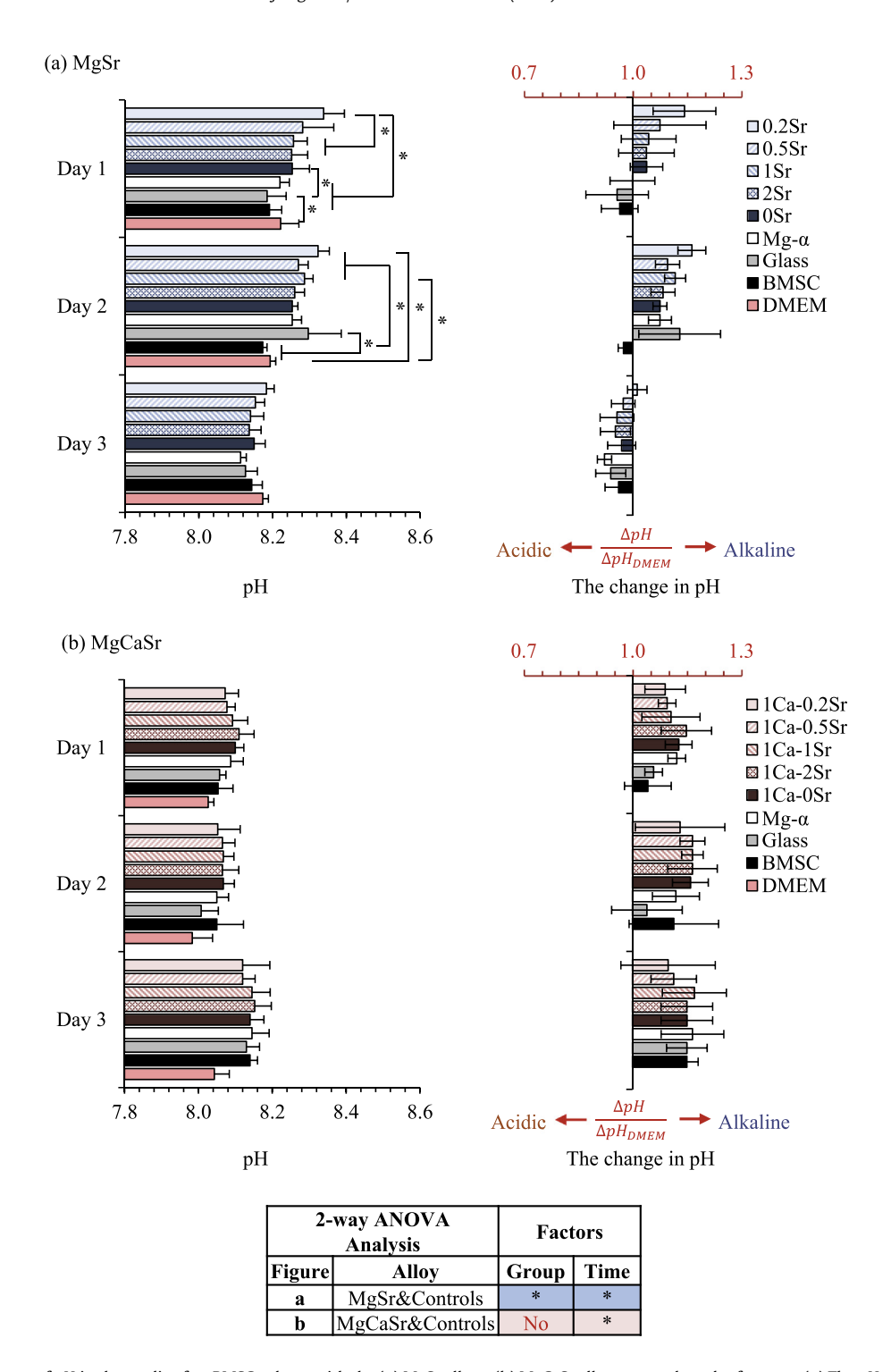


Fig. 5. The pH and the change of pH in the media after BMSC culture with the (a) MgSr alloys, (b) MgCaSr alloys, controls and references. (a) The pH and the change of pH in the media after BMSC culture with MgSr alloys and controls. (b) The pH and the change of pH in the media after BMSC culture with MgCaSr alloys, controls and references. The change in pH shown in (a) and (b) were normalized by the mean change of pH in the media of DMEM reference group at each prescribed time point. The table shows the 2-way ANOVA analysis of dependency of media pH on group and time. Values are mean ± standard deviation (n = 3). *p < 0.05.

contact condition (i.e., cells attached on the culture plate around the samples). In the fluorescence images, all the groups showed confluent BMSCs covering almost the entire culture plate around each sample. Fig. S1f shows the cell adhesion density in the indirect contact condition normalized by the cell adhesion density in the BMSC reference, namely cell density ratio. No statistically significance was detected among all the groups, and 0.2Sr showed lower cell density ratio than the other groups in average.

3.6. Characterization of cell-material interface

Fig. 7 shows the morphologies of BMSCs and microstructure of MgSr alloys and pure Mg controls of 0Sr and Mg- α at the interface in the SEM images, and the overlaid SEM images with EDS elemental maps (SEM + EDS) for each group. The respective EDS maps for carbon and calcium are shown in two separate channels in the right two columns of Fig. 7. In the SEM + EDS, EDS (carbon) and

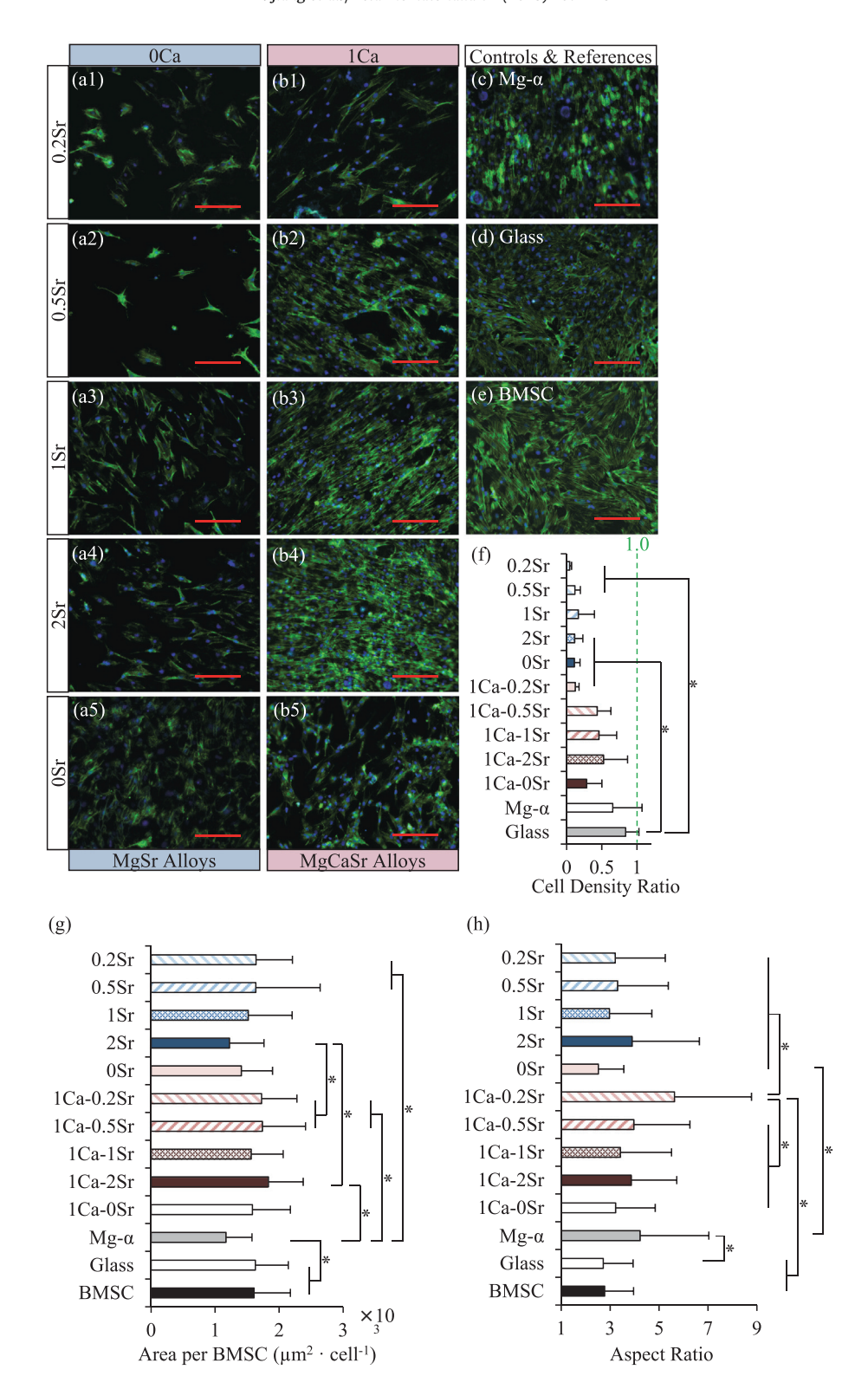


Fig. 6. Fluorescence images and the quantitative analysis of BMSCs directly attached on the MgSr alloys, MgCaSr alloys, controls and references (i.e., direct contact) after *in vitro* culture for 72 h. The fluorescence images of (a1–a4) MgSr alloys, (a5) 0Sr control, (b1–b4) MgCaSr Alloys, (b5) Mg-1Ca control, and Mg-α control, glass and BMSC references. F-actin was stained with Alexa Fluor. 488 phalloidin as indicated by green color. Cell nucleus was stained with DAPI as indicated by blue color. The green dash line represents the ratio = 1. Scale bar = 200 μm, original magnification = 100x. The bar graphs show (f) the ratio of the adhesion density of BMSCs on respective samples normalized by the mean adhesion density of BMSC reference, (g) spreading area per BMSC, and (h) aspect ratio of BMSCs. Values are mean ± standard deviation (n = 3). p < 0.05. (For interpretation of the references to color in this figure legend, the reader is referred to the web version of this article.)

EDS (calcium) maps, each color represents a different element as shown in the legend. All the MgSr alloys and pure Mg controls of OSr and Mg- α showed corrosion cracks on their surfaces. Visually, the four MgSr alloys appeared to have distinct microstructures on

their surface layers. The cracks in 0.5Sr, 1Sr and 0Sr control were much wider than all the other groups. The locations of BMSCs in the SEM images overlapped with the regions of intensified C distribution in the EDS maps, which indicated that the C element came

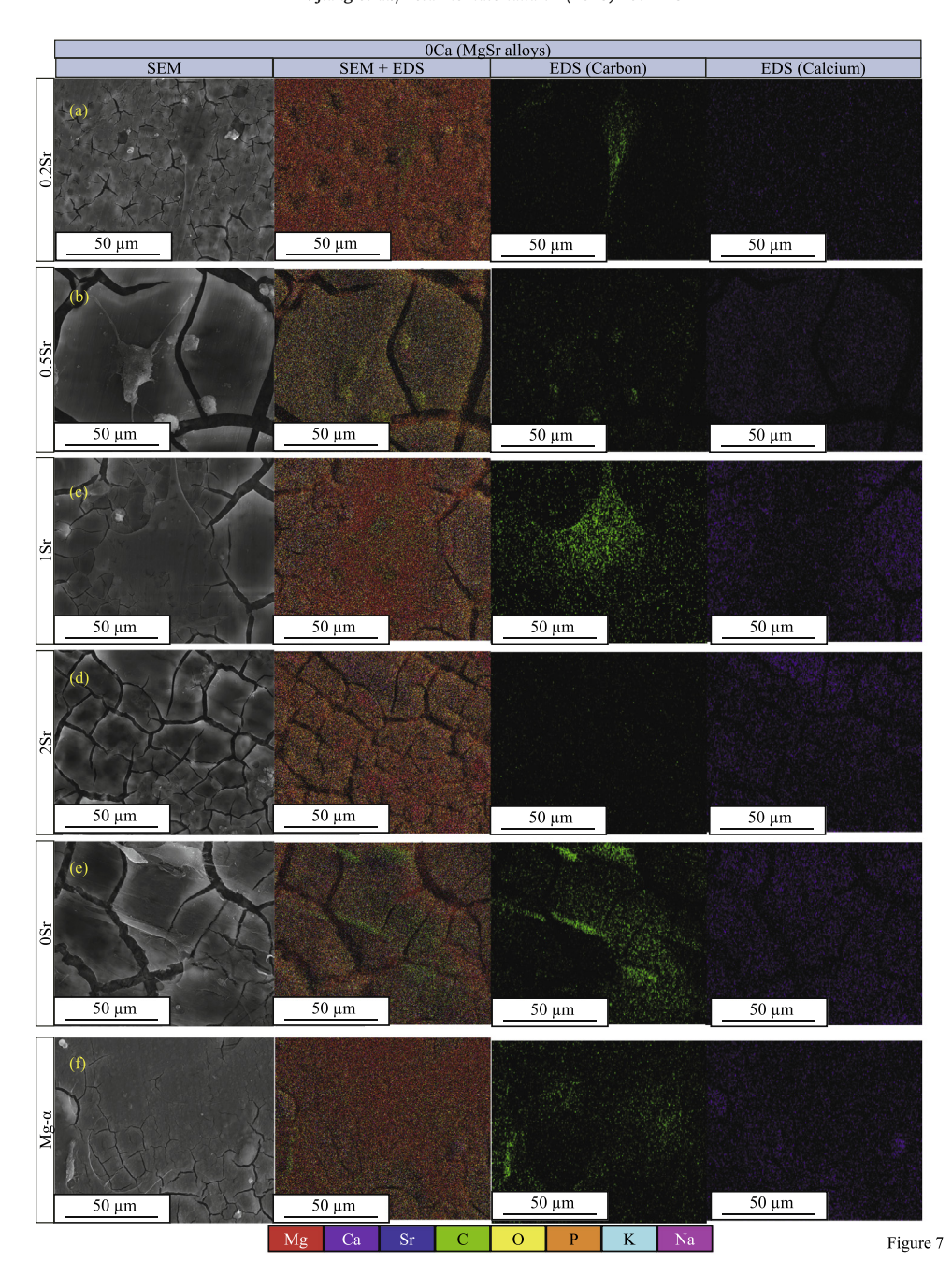


Fig. 7. Surface morphologies and elemental distribution of (a–d) MgSr alloys, (e) OSr control, and (f) Mg- α control with the direct-contact BMSCs after 72 h of culture. SEM images (SEM column) show the surface morphologies and cell morphologies; and the overlaid SEM and EDS maps (SEM + EDS column) show the key elemental distributions by color maps on the respective surface. The distributions of carbon and calcium measured using EDS are also shown in separate columns. Scale bar = 50 μm, original magnification = $1000 \times$.

from the cells. None of the four MgSr alloys showed obvious correlations between the distribution of Ca element and C element on their surfaces; Ca seemed to distribute homogenously on the surface except around the cracks and the regions shielded by BMSCs (e.g. 1Sr in Fig. 7).

Fig. 8 shows the morphologies of BMSCs and microstructure of MgCaSr alloys, 1Ca-0Sr control and glass control at the interface in the SEM images, and the overlaid SEM images with EDS elemental maps (SEM + EDS) for each group. The respective EDS maps for carbon and calcium are shown in two separate channels in the right two columns of Fig. 8. The overlaid images, Ca maps and C maps of all MgCaSr alloys (except for 1Ca-2Sr) and 1Ca-0Sr control

showed Ca element distributed at certain locations, and some Ca located around the sites of BMSC attachment in their respective SEM images. 1Ca-2Sr showed that the Ca element distributed homogeneously over the entire image.

Fig. 9 shows the morphologies of individual BMSC in direct contact with MgSr alloys and MgCaSr alloys on their surfaces. Fig. 9a1 shows the morphology of a BMSC attached on the surface of 0.2Sr, which appeared to be more spreading. Fig. 9a2 shows the morphology of a BMSC attached on the surface of 0.5Sr, which demonstrated a less spreading cell morphology. Fig. 9a3 shows the morphology of a BMSC attached on the surface of 1Sr, which appeared to be spreading widely. Fig. 9a4 shows the surface of

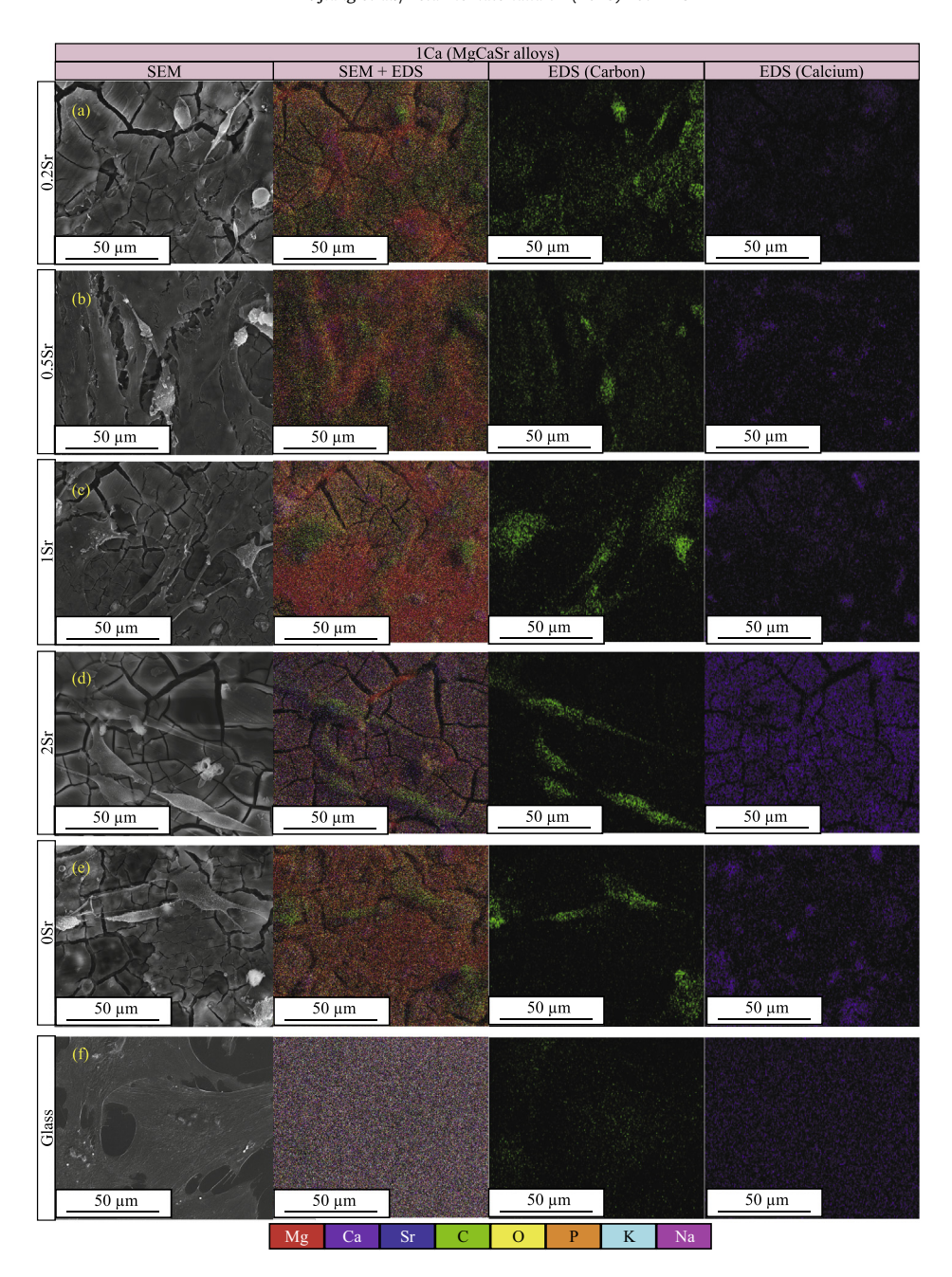


Fig. 8. Surface morphologies and elemental distribution of (a–d) MgCaSr alloys, (e) 1Ca-OSr control, and (f) glass reference with the direct-contact BMSCs after 72 h of culture. SEM images (SEM column) show the surface morphologies and cell morphologies; and the overlaid SEM and EDS maps (SEM + EDS column) show the key elemental distributions by color maps on the respective surface. The distributions of carbon and calcium measured using EDS are also shown in separate columns. Scale bar = $50 \mu m$, original magnification = $1000 \times$.

2Sr, but no BMSC was found. Fig. 9b1 shows a BMSC attached on the surface of 1Ca-0.2Sr with a highly elongated but less spreading morphology. Fig. 9b2 shows a BMSC attached on the surface of 1Ca-0.5Sr had a slightly elongated morphology that is less spreading. Fig. 9b3 shows a BMSC attached on the surface of 1Ca-1Sr was spreading at multiple directions, but it still presented a poorly spreading cell morphology. Fig. 9b4 shows a BMSC attached on the surface of 1Ca-2Sr with elongated but less spreading morphology. Compared with the BMSCs attached onto binary MgSr alloys, the BMSCs attached on ternary MgCaSr alloys appeared to have less spreading morphologies while the BMSCs on binary MgSr alloys appeared to have more spreading morphologies. Fig. 9c1 shows a BMSC attached on the pure Mg control of 0Sr with a less

spreading morphology. Fig. 9c2 shows round and poorly spread BMSCs attached on the surface of the pure Mg control of Mg- α .

4. Discussion

- 4.1. Degradation of MgSr alloys and MgCaSr alloys in vitro
- 4.1.1. The relationship between degradation rates and composition of MgSr or MgCaSr alloys

The varying Ca and Sr content in the Mg alloys profoundly affected the degradation rates of the alloys. Specifically, the elemental compositions will determine the alloying phase

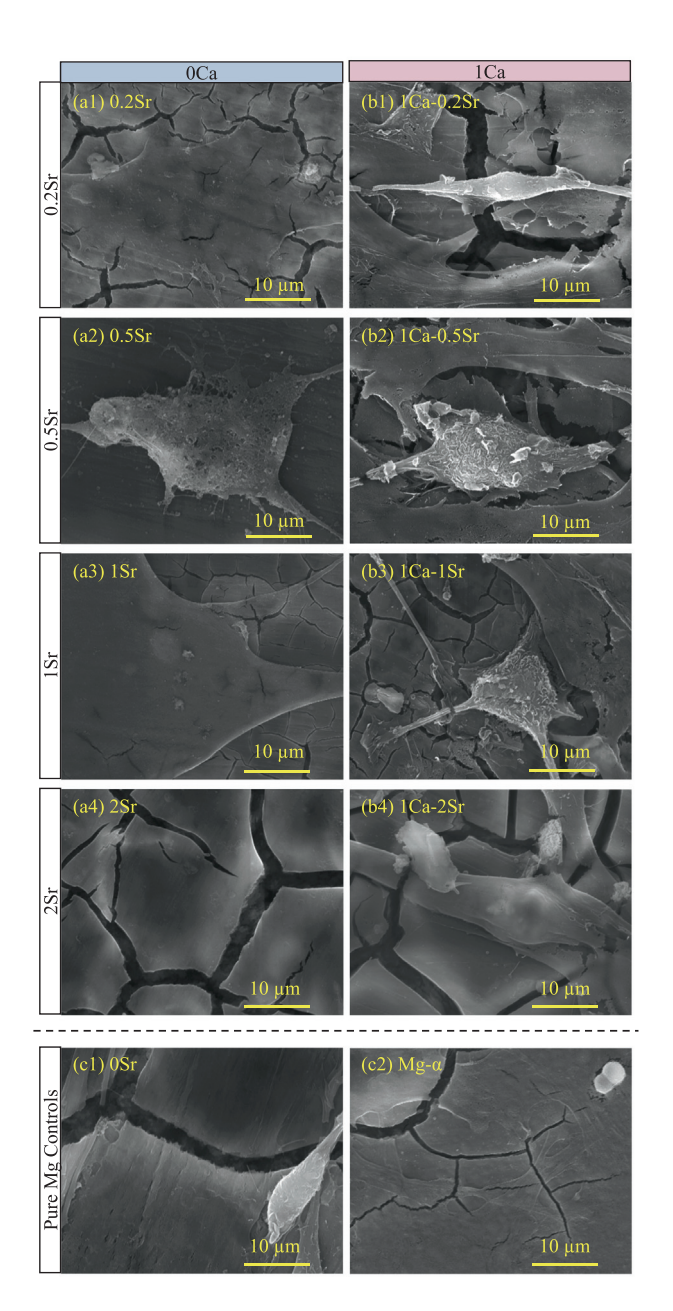


Fig. 9. SEM images showing the morphologies of individual BMSC directly attached on the surface of (a1–a4) MgSr alloys, (b1–b4) MgCaSr alloys, (c1–c2) pure Mg controls of (c1) OSr and (c2) Mg- α after 72 h of direct culture. No BMSC was found on Mg-2Sr alloy. Scale bar for all images = 10 μ m, original magnification for all images = 1000 \times .

compositions and microstructures when the alloys were processed and heat-treated with the same procedures. The different phases and microstructures have different corrosion potentials, and thus affect the degradation rates of Mg alloys. In this study, the neutralizing effect of Ca on the Sr-dependent degradation rates (Fig. 4) could be associated with the different phase compositions in the MgSr alloys and MgCaSr alloys. For Mg-Sr system, it was theoretically predicted that Mg-0.2Sr and Mg-0.5Sr could consist of Mg matrix and Mg₁₇Sr₂ phase [35]. If Sr content increases to 1 wt% as in Mg-1Sr, Mg₃₈Sr₉ phase could totally replace Mg matrix and co-exist with Mg₁₇Sr₂ [35]. When Sr content increases to 2 wt%, the phase composition could change to Mg₂₃Sr₆ and Mg₂Sr [35]. Interestingly, XRD results from other studies supported that the

increase of Sr content from 0 wt% to 4 wt% resulted in a larger faction of the Mg₁₇Sr₂ phase, not the Mg₂₃Sr₆ phase [22,36]. The increase of Mg₁₇Sr₂ phase was believed to be responsible for the faster corrosion rates of Mg alloys with higher Sr percentage because it formed a galvanic couple with α -Mg [22]. Although different reports did not agree perfectly on the microstructures of MgSr alloys, possibly because of variations in their alloy processing parameters, they all suggested that the addition of Sr element from 0.2 wt% to 2 wt% could induce drastic transition of phases and microstructures, and consequently led to the change of degradation rates [22,35,36]. In contrast, the ternary Mg-Ca-Sr system was reported to have a more stable phase composition consisting of Mg matrix, Mg₁₇Sr₂ phase and C14 phase which can contain both Mg₂Sr and Mg₂Ca sublattices [35]. Interestingly, Sr and Ca atoms can freely replace each other in C14 phase due to their similar atomic sizes [35]. This special C14 phase in MgCaSr alloys appears to be the reason of the stabilizing effects of Ca element. With increasing Sr content, Mg-1Ca-xSr is likely to have increasingly more Mg₂Sr sublattice over Mg₂Ca sublattice, but it may undergo little phase change due to the similarity between the two sublattices. This stabilized phase composition was also confirmed in another experimental study where Mg-1Ca-0.5Sr kept the phase composition of Mg, Mg₂Ca and Mg₁₇Sr₂ unchanged, when the Sr content was doubled from 0.5 wt% to 1.0 wt% [37]. As a result, MgCaSr alloys did not show significant change in degradation rates with increasing Sr content (Fig. 4).

Although the presence of Ca could neutralize the effects of different Sr content on the degradation rates of Mg alloys (Fig. 4), it will also lead to the formation of Mg₂Ca phase which is detrimental to the corrosion resistance of MgCaSr alloys. It was previously reported that adding Ca element can accelerate the degradation of Mg by forming Mg₂Ca intermetallic phase which has higher corrosion current density than α -Mg phase [38], and the formation of Mg₂Ca phase could have occurred during the melting process at 720 °C, according to theoretical prediction [39] and experimental report [37]. This mechanism could be the major factor that placed the corrosion resistance of MgCaSr alloys in the middle of the lessresistant 0.2Sr and the more-resistant 1Sr and 2Sr. 1Sr and 2Sr were found to have the lowest degradation rates among all MgSr and MgCaSr alloys in this study. Lastly, it should be noted that the alloys fabricated in this study contained trace amount of impurities. The raw materials used to fabricate the alloys were the 99.7% pure Mg, 99.8% pure Ca, and 99.9% pure Sr. The impurities from the source materials could also affect the corrosion properties of the alloys.

4.1.2. Electrochemical testing versus immersion degradation in BMSC/DMEM culture

The improved electrochemical corrosion resistance of 1Sr and 2Sr (Fig. 2a2) was consistent with their reduced in vitro degradation rates during immersion in BMSC culture (Fig. 4), but the electrochemical corrosion behaviors of 1Ca-1Sr and 1Ca-2Sr did not agree well with the respective in vitro degradation rates in the BMSC/DMEM direct culture system (i.e., direct culture of Mg alloys with BMSCs in DMEM, as defined in [29]). The 1Ca-1Sr and 1Ca-2Sr showed better electrochemical corrosion resistance than the other MgCaSr alloys and Mg- α control (Fig. 2b2), but their degradation rates in the BMSC/DMEM direct culture system showed no statistically significant difference when compared with the other MgCaSr alloys and Mg- α control (Fig. 4). It should be noted that the behaviors of in vitro degradation in immersion could be different from the corrosion behaviors measured by electrochemical method for several reasons. Generally, the corrosion resistance determined by potentiodynamic polarization method is considered as an estimate based on the initial electrochemical behaviors of Mg alloys, whereas the in vitro degradation measured by immersion in the

cell culture system over a longer period of time is considered to be able to project the in vivo degradation more closely [16,30,40]. In contrast to the electrochemical measurements in rSBF, the immersion degradation in the BMSC/DMEM direct culture system takes the influence from the cells and proteins into account. Previous studies have shown that the presence of cells and proteins could lead to significant changes in Mg alloy degradation [29,41-46]. Moreover, some differences in environmental factors could also play a role in the degradation results of Mg alloys. For example, potentiodynamic measurements was typically performed in air where CO₂ content is around 0.4%, while the degradation in BMSC/DMEM culture typically occurs under the standard cell culture conditions where 5% CO2 was maintained. As previously reported, CO₂ played a critical role in the process of Mg degradation [29,41,47], because CO₂ could lead to the formation of H₂CO₃, which could induce more precipitation of MgCO₃ [47]. Additionally, the HCO₃ ion concentration in the BMSC/DMEM direct culture system (44.04 mM) is much higher than in that of rSBF (27 mM), which could affect the degradation of Mg alloys. Lastly, the presence of g-glucose in the BSMC/DMEM system could also have a considerable contribution to the discrepancy between the degradation rates measured in the BMSC/DMEM direct culture and the corrosion properties measured by the electrochemical method [29.41]. Based on these reasons, the PDP method following ASTM standard (G102-89) should be used as a complementary characterization to understand the electrochemical corrosion resistance of Mg alloys; and the results of immersion degradation in the direct culture with cells should be considered as a better prediction of the degradation properties of Mg alloys in vivo.

4.1.3. The variations in the Mg^{2+} , Sr^{2+} , and Ca^{2+} concentrations in the BMSC/DMEM culture with MgSr alloys, MgCaSr alloys, controls and references

The concentrations of metallic divalent ions were critical to understand the degradation process of Mg alloys in the BMSC/ DMEM direct culture system. The Mg²⁺ ion in the culture with all MgSr alloys, MgCaSr alloys and controls showed higher Mg²⁺ ion concentrations than their references (Fig. 3a1 and 3b1), which was apparently caused by the degradation of Mg alloys. However, the lower Ca²⁺ ion concentrations in the media of all MgCaSr alloys at day 1 and day 2 (Fig. 3b3) indicated a more complicated degradation process. The degradation itself should have released more Ca²⁺ ion into the media, but the increase of Mg²⁺ ion concentration in their media as compared with references (Fig. 3b1) could facilitate the precipitation of Ca²⁺ ion onto sample surface. Mg²⁺ ion was reported to induce mineral deposition in the form of Ca-containing salts in alkaline environment [21,48,49]. Thus, the significant decrease of Ca²⁺ ion concentrations in the cultures with MgCaSr alloys at day 1 and day 2 could be the result of Mg-induced Ca deposition, and the increase of Ca2+ ion concentrations back to the same level as controls at day 3 may indicate that the Ca deposition was counteracted by the Ca release from the MgCaSr alloys at day 3.

The Sr²⁺ ion concentrations in the media of both MgSr alloys and MgCaSr alloys were apparently affected by the Sr content in the alloys (Fig. 3a2 and 3b2). The increasing Sr content could have resulted in the formation of more Sr-rich phases, such as Mg₂Sr and Mg₂₃Sr₆ which were previously discussed in 4.1.1. The degradation of Sr-rich phases could have significantly increased the Sr²⁺ ion concentrations in the media. The drastically varying Sr²⁺ ion concentrations for 1Ca-2Sr (Fig. 3b2) could be possibly ascribed to its inhomogeneous phase distribution or the degradation layer on sample surfaces. However, this is merely a speculation, and further investigation on the bulk phase distribution and surface phase composition of 1Ca-2Sr is needed.

4.1.4. The change of the pH in the BMSC/DMEM culture with MgSr alloys, MgCaSr alloys, controls and references

The pH change in the media was associated with the degradation of MgSr and MgCaSr alloys. The degradation of MgSr alloys tended to alkalize the culture media at day 1 and day 2 (Fig. 5a). However, the trend seemed to start reversing to the more acidic direction at day 3 (Fig. 5a). This result could be explained by the reduced rates of degradation of MgSr alloys over time (Fig. 4). According to Eq. (1) [34], the produced OH⁻ during the degradation was a dominant factor to alkalize the culture media, and the rate of this degradation reaction was decreasing from day 1 to day 3 (Fig. 4). At day 3, the alkalizing effect was outpaced by the acidizing effect (Fig. 5a), i.e. possibly the buffering effect of the culture media and the cell metabolic activities. In contrast, MgCaSr alloys kept a stable alkalizing tendency over 3 days (Fig. 5b), possibly because their degradation rates did not decrease during the entire 3-day culture (Fig. 4). In addition, the stabilizing effects of Ca elements as discussed in 4.1.1 could possibly result in the minimal change of pH among all MgCaSr alloys at each day (Fig. 5).

4.2. Factors that affected BMSC behaviors in the direct and indirect contact

The adhesion density of BMSCs on MgCaSr alloys (Fig. 6) indicated that MgCaSr alloys could provide better cytocompatibility and less toxicity than MgSr alloys. As expected, the glass control showed greater BMSC adhesion density than all Mg alloys of interest, because glass controls are widely used as a positive control in cell cultures and often showed favorable adhesion of BMSCs on the surface [16,18,29]. The objective of this cell study was to compare the cytocompatibility of MgSr and MgCaSr alloys and to screen for the most promising candidates toward *in vivo* studies and preclinical trials in the future.

Surface roughness and grain size could affect the cell adhesion and function on the surfaces of Mg alloys. In this study, all the Mg-based samples were grinded and polished using SiC paper up to 1200 grit before cell culture, which should result in consistent and similar surface roughness for all samples. Therefore, surface roughness was not likely to be the main responsible factor for the observed differences in BMSC adhesion and spreading on the different Mg alloy groups and pure Mg controls (Fig. 6). Our previous study indicated that the Mg-Sr alloys exhibited finer grain sizes with increasing Sr content [22]. The average grain size was 32.3 \pm 6.7 μm for Mg-1Sr and 25.9 \pm 8.3 μm for Mg-2Sr [22]. The refined grain sizes might have contributed to the improved BMSC adhesion on Mg-1Sr and Mg-2Sr samples when compared with Mg-0.2Sr and Mg-0.5Sr samples (Fig. 6).

The improved BMSC adhesion on the surfaces of MgCaSr alloys in comparison with MgSr alloys (Figs. 6-8) could be a result of Ca presence on the surfaces of MgCaSr alloys (Fig. 8). The aggregated Ca element can be clearly observed on the surface of 1Ca-0.5Sr, 1Ca-1Sr and 1Ca-0Sr (Fig. 8), which was likely deposition of Cacontaining minerals. The Ca-containing minerals on the surface possibly created a more bone-mimicking interface where BMSCs were attracted to attach and spread. On the surfaces of MgCaSr alloys, Ca element aggregated around but not overlapped with the C-rich region which was likely the sites of BMSC attachment in the corresponding SEM + EDS image (Fig. 8). Previous reports showed that the Mg metal could catalyze the formation of minerals such as hydroxyapatite [50,51]. The formation of Ca-containing minerals could have provided favorable sites for BMSCs to attach. Similar incorporation of Ca on surface was previously reported to promote the cell adhesion on both Mg alloys [21] and Ti alloys [52,53]. It should be noted that Ca element on the surfaces of MgCaSr alloys could have also originated from the pre-existed Ca in the original alloys. MgCaSr alloys contain 1 wt% of Ca, which could account for the Ca presence on their surfaces, especially on the surface of 1Ca-2Sr where Ca elements distributed ubiquitously all over the surface (Fig. 8). More likely, Ca on the surface was the reason for improved BSMC adhesion rather than the result of BMSC adhesion, i.e. Ca on the surface promoted BMSC activities, not that the BMSC induced the aggregation of Ca elements. The dominating Ca deposition from culture media was most possibly induced by Mg-based samples through Ca-containing mineral deposition process [30], less likely by the BMSCs. The evidence lied in our observation that no significant difference in Ca²⁺ ion concentrations was found in the media of the BMSC reference group and DMEM reference group (Fig. 3b3), suggesting the presence of BMSCs did not induce significant variations in Ca content. This speculation is in agreement with another study with human endothelial cells that showed no significant change in Ca2+ ion concentrations when comparing the cell-only reference with the media-only reference [30]. Even if BMSCs released intracellular Ca, it would not be sufficient to make a noticeable difference in Ca2+ ion concentration in the media. In fact, the intracellular Ca level for most cells is considerably low $(0.1-1 \mu M [54])$ as compared with Ca level in culture media (1-2 mM, as shown in Fig. 3b3). Thus, the influence of BMSCs on Ca content in the media or on alloy surfaces should be very limited. Based on these evidences, we believe that preexisted Ca in the MgCaSr alloys and the presence of Ca-rich sites on the surface could have promoted BMSC adhesion on its surface.

The decrease of Ca²⁺ ion concentration in the culture media (Fig. 3b3) could also contribute to the improved BMSC adhesion on the surface of MgCaSr alloys (Figs. 6–8). The Ca²⁺ could inhibit cell adhesion when its concentration exceeds 1 mM [55-63], and hence the decrease of Ca²⁺ ion concentration in the culture media could reduce the suppressing effect of Ca2+ on the adhesion of BMSCs. It is noteworthy that the adhesion density of BMSCs under indirect contact conditions was not significantly affected by Ca²⁺ ion concentration (See Fig. S1 in Supplementary Materials). The Ca-containing mineral deposition occurred near the surface of the samples, and thus Ca²⁺ ion concentration near the sample surface could be even lower than the whole culture well. Similar gradient effect of ion concentration was also reported elsewhere [64]. Lastly, at day 3, the Ca²⁺ ion concentration in all groups returned to the same level (Fig. 3b3). Thus, the adversary effects of Ca²⁺ ions on the BMSC adhesion on plate was mitigated due to the decrease of Ca²⁺ ion concentrations in the culture media, which avoided the inhibitory effects of BMSC adhesion on MgCaSr alloys to a degree

BMSC adhesion was possibly associated with Sr²⁺ ion concentrations in the media as well. The groups of 0.2Sr and 1Ca-0.2Sr showed lower BMSC adhesion on surface (Fig. 6) as compared with their high Sr-content counterparts that showed more Sr²⁺ present in the media (Fig. 3a2 and 3b2). However, this Sr²⁺-dependent change of BMSC adhesion density is complicated by the presence of Mg²⁺ and Ca²⁺ which could also greatly affect BMSC activities. Indeed, although 1Ca-0.5Sr showed slightly fewer Sr²⁺ ion in the media (~2.1 $\mu M)$ than 1Ca-0.2Sr (~2.5 $\mu M)$ as shown in Fig. 3b2, its BMSC adhesion density was strikingly higher than 1Ca-0.2Sr and was comparable to 1Ca-2Sr (Fig. 6) whose media contained drastically higher Sr^{2+} ion concentration ($\sim 6.1 \, \mu M$, as shown in Fig. 3b2). The correlation between Sr²⁺ ion concentration and BMSC adhesion density is not conclusive, but possible. In addition, for 1Ca-0.2Sr and 1Ca-2Sr showed a higher Sr²⁺ ion concentrations in BMSC culture media at day 1 and day 3; and the BMSCs attached on their surfaces showed more elongated cell morphology than 1Ca-0.5Sr and 1Ca-1Sr. Thus, the high Sr²⁺ ion concentrations in the culture media of 1Ca-2Sr could have improved the spreading of BMSCs. To our knowledge, Sr²⁺ ion has beneficial effects on bone-relevant cell adhesion and functionality. Sr2+ ion was reported to enhance proliferation and alkaline phosphatase (ALP) activity of osteoblasts [65]. It was also shown to upregulate the ALP activity and gene expressions of collagen I (COL1A1), bone sialoprotein (BSP) and RUNX2 of Saos-2 osteosarcoma cells [66]. Unfortunately, the molecular mechanism of Sr²⁺ ion participating in cell adhesion has not been systematically investigated [16]. Mg²⁺, Ca²⁺ and Mn²⁺ are the most investigated divalent ions, and they all played critical roles on the functions of integrins [55-63]. Despite of the similarity of Sr²⁺ to Ca²⁺, whether or not Sr²⁺ could have a similar effect on integrin functions remains unclear. In contrast to Ca²⁺ ions, higher concentration of Sr²⁺ ions may not necessarily lead to negative effects on BMSCs. Excessive Ca²⁻ ions will pressure the cells to consume energy to maintain a stable intracellular Ca level [55-63], and this Ca-specific mechanism may not apply to Sr²⁺ ion. A previous study observed Sr-substituted hydrogel could have more favorable effects on cells than Casubstituted gel [66], which supported our speculation.

The degradation rates of Mg alloys could have also played an important role in affecting BMSC adhesion directly on sample surface. Our results indicated that the rapid degradation of 0.2Sr was associated with its lower adhesion density of BMSCs (Fig. 4 and Fig. 6) on its surface. Similarly, the poor BMSC adhesion on the surface of 1Ca-0.2Sr (Fig. 6) could be a result of its rapid degradation at day 3 (Fig. 4). The rapid degradation was reported to induce local alkalinity [64]; the adhesion of BMSCs could be inhibited by the aggressive degradation occurring at the interface of Mg alloys and BMSCs. In addition, the hydrogen gas (H₂) produced during the degradation could be another factor that influenced BMSC activities. H₂ gas causes concerns in the clinical use because the accumulation of excess amount of H₂ gas could impair the quality of newly-formed bone [16]. The evolution of H₂ was not measured directly in our direct culture experiment, considering that H₂ is produced at a rate theoretically proportional to the release of Mg^{2+} ions, according to Eq. (1) [34]. We did not collect and measure the amount of H₂ evolution to avoid the potential disruption on the BMSC activities. However, H₂ is not a negligible factor in the direct culture. Rapid degradation of a Mg alloy should have resulted in a faster H₂ gas evolution while slower degradation of a Mg allov should release less H₂ gas, which may affect BMSC activities.

The BMSCs on the surface of MgSr and MgCaSr alloys showed a decreasing trend of spreading area per cell with increasing Sr content at the fixed Ca content (Fig. 6g), which was in reverse to the adhesion density (Fig. 6f). We speculated that the denser BMSC distribution on the high-Sr alloy surfaces limited the space for BMSCs to sufficiently spread. In fact, the BMSCs on the surface of 1Ca-0.5Sr, 1Ca-1Sr and 1Ca-2Sr (Fig. 6b2~6b4) showed a nearly 100%c ell coverage. A significant number of BMSCs were visually observed to overlap with their neighboring BMSCs (Fig. 6b2–6b4). In addition, no obvious trend of aspect ratio was found except for the statistically higher aspect ratio for 1Ca-0.2Sr than all the other MgCaSr alloys and MgSr alloys (Fig. 6h). The elongated morphology of individual BMSC was observed (Fig. 9b1), which agrees very well with the high aspect ratio measured for the cells on 1Ca-0.2Sr (Fig. 6h).

For BMSCs attached on the plate surrounding the samples (indirect contact), the difference in BMSC adhesion density among different groups was negligible since no statistically significant difference was found (see Fig. S1 in supplementary materials), suggesting that the release of soluble ions such as Mg²⁺ ions, Ca²⁺ ions, Sr²⁺ ions, and OH⁻ ions from the MgSr and MgCaSr alloys of interest and the released H₂ gas in the culture plate did not harm BMSCs. Although the Mg²⁺ ion concentrations in the culture media and the media pH varied by groups, none of them increased to the level harmful to BSMCs. Previous studies showed that Mg²⁺ ion concentrations up to 27.6 mM and transient media pH up to 9.0 did not induce adverse effects on BMSCs [18]. In this study, the highest Mg²⁺ ion concentration in the culture media was below

3.5 mM (Fig. 3a1 and 3b1), and the highest pH in the culture media was below 8.4 (Fig. 5a and 5b), thus unlikely to have adverse effects on the adhesion of BMSCs. The highest Sr^{2+} ion concentration in this study (8.2 μ M, as shown in Fig. 3b2) was still much lower than the lethal dosage (LD50) of Sr^{2+} (33.8 mM [67,68]). To clarify, all the ion concentrations could be higher at the surface of Mg alloys due to the dynamic degradation reactions, and thus could affect BMSCs in direct contact with the alloy surfaces. However, under the indirect contact conditions of the direct culture, soluble degradation products from the MgSr and MgCaSr alloys did not cause any detectable harm to BMSCs.

5. Conclusions

This study screened and comparatively investigated the *in vitro* degradation and cytocompatibility of four different binary MgSr alloys and four different ternary MgCaSr alloys. Mg-1Sr and Mg-2Sr were identified to have the lowest degradation rates among all MgSr and MgCaSr alloys studied. MgCaSr alloys generally showed an improved BMSC adhesion on their surfaces as compared with MgSr alloys, except for Mg-1Ca-0.2Sr. Collectively considering the degradation properties (rate and mode) and BMSC behaviors, Mg-1Sr, Mg-1Ca-0.5Sr and Mg-1Ca-1Sr are recommended for further *in vivo* studies in animal models toward clinical translation.

Acknowledgements

The authors thank the U.S. National Science Foundation (CBET 1512764), U.S. National Institute of Arthritis and Musculoskeletal and Skin Diseases (NIAMS) of the National Institutes of Health (Award 1R03AR069373), University of California (UC) Regents Faculty Fellowship (H.L.) and Faculty Development Award (H.L.), Hellman Faculty Fellowship (H.L.), UC-Riverside (UCR) Academic Senate Seed Grant (H.L.), and National Natural Science Foundation of China Grant No. 51431002 (Y.Z.) for financial support. The authors thank the UCR Graduate Division for Dissertation Year Fellowship (A.F.C.) and Dissertation Research Grant (Q.T. and W.J.). The authors thank the following programs for supporting undergraduate student researchers: California Institute for Regenerative Medicine (CIRM) Bridges to Stem Cell Research Program (A.S.), Hispanic Serving Institution STEM Pathway Program (A.L.), Mentoring Summer Research Internship Program (MSRIP) at UCR (M.L., M.C.), and Maximizing Access to Research Careers Undergraduate Student Training in Academic Research (MARC U-STAR) Program (U. S. National Institute of Health training grant T34GM062756) (M. C.). The authors thank Central Facility for Advanced Microscopy and Microanalysis (CFAMM) at UCR for the usage of SEM and EDS. The authors thank UCR Bioengineering undergraduate researcher Ammar Dilshad Hakim for helping with Fig. 1 illustration. The content is solely the responsibility of the authors and does not necessarily represent the official views of the National Institutes of Health and National Science Foundation.

Appendix A. Supplementary data

Supplementary data associated with this article can be found, in the online version, at https://doi.org/10.1016/j.actbio.2018.03.049.

References

- [1] Q. Tian, H. Liu, Electrophoretic deposition and characterization of nanocomposites and nanoparticles on magnesium substrates, Nanotechnology 26 (17) (2015) 175102.
- [2] H. Zreiqat, C.R. Howlett, A. Zannettino, P. Evans, G. Schulze-Tanzil, C. Knabe, M. Shakibaei, Mechanisms of magnesium-stimulated adhesion of osteoblastic cells to commonly used orthopaedic implants, J. Biomed. Mater. Res. 62 (2) (2002) 175–184.

- [3] F. Witte, N. Hort, C. Vogt, S. Cohen, K.U. Kainer, R. Willumeit, F. Feyerabend, Degradable biomaterials based on magnesium corrosion, Curr. Opin. Solid State Mater. Sci. 12 (5–6) (2008) 63–72.
- [4] N.E. Saris, E. Mervaala, H. Karppanen, J.A. Khawaja, A. Lewenstam, Magnesium. An update on physiological, clinical and analytical aspects, Clinica Chimica Acta; Int. J. Clin. Chem. 294 (1–2) (2000) 1–26.
- [5] M.P. Staiger, A.M. Pietak, J. Huadmai, G. Dias, Magnesium and its alloys as orthopedic biomaterials: a review, Biomaterials 27 (9) (2006). 1728 34.
- [6] H. Waizy, J.-M. Seitz, J. Reifenrath, A. Weizbauer, F.-W. Bach, A. Meyer-Lindenberg, B. Denkena, H. Windhagen, Biodegradable magnesium implants for orthopedic applications, J. Mater. Sci. 48 (1) (2012) 39–50.
- [7] H.S. Brar, M.O. Platt, M. Sarntinoranont, P.I. Martin, M.V. Manuel, Magnesium as a biodegradable and bioabsorbable material for medical implants, JOM US 61 (9) (2009) 31–34.
- [8] A.F. Cipriano, A. Sallee, R.G. Guan, A. Lin, H.N. Liu, A Comparison Study on the Degradation and Cytocompatibility of Mg-4Zn-xSr Alloys in Direct Culture, ACS Biomater. Sci. Eng. 3 (4) (2017) 540–550.
- [9] D.W. Zhao, F. Witte, F.Q. Lu, J.L. Wang, J.L. Li, L. Qin, Current status on clinical applications of magnesium-based orthopaedic implants: a review from clinical translational perspective, Biomaterials 112 (2017) 287–302.
- [10] A.H.M. Sanchez, B.J.C. Luthringer, F. Feyerabend, R. Willumeit, Mg and Mg alloys: How comparable are in vitro and in vivo corrosion rates? a review, Acta Biomater. 13 (2015) 16–31.
- [11] X.J. Wang, D.K. Xu, R.Z. Wu, X.B. Chen, Q.M. Peng, L. Jin, Y.C. Xin, Z.Q. Zhang, Y. Liu, X.H. Chen, G. Chen, K.K. Deng, H.Y. Wang, What is going on in magnesium alloys?, J Mater. Sci. Technol. (2017).
- [12] Y.F. Ding, C.E. Wen, P. Hodgson, Y.C. Li, Effects of alloying elements on the corrosion behavior and biocompatibility of biodegradable magnesium alloys: a review, J. Mater. Chem. B 2 (14) (2014) 1912–1933.
- [13] S. Bagherifard, D.J. Hickey, S. Fintová, F. Pastorek, I. Fernandez-Pariente, M. Bandini, T.J. Webster, M. Guagliano, Effects of nanofeatures induced by severe shot peening (SSP) on mechanical, corrosion and cytocompatibility properties of magnesium alloy AZ31, Acta Biomater. 66 (2018) 93–108.
- [14] M. Peron, J. Torgersen, F. Berto, Mg and Its alloys for biomedical applications: exploring corrosion and its interplay with mechanical failure, Met. Basel 7 (7) (2017).
- [15] F. Witte, V. Kaese, H. Haferkamp, E. Switzer, A. Meyer-Lindenberg, C.J. Wirth, H. Windhagen, In vivo corrosion of four magnesium alloys and the associated bone response, Biomaterials 26 (17) (2005) 3557–3563.
- [16] A.F. Cipriano, A. Sallee, M. Tayoba, M.C.C. Alcaraz, A. Lin, R.G. Guan, Z.Y. Zhao, H.N. Liu, Cytocompatibility and early inflammatory response of human endothelial cells in direct culture with Mg-Zn-Sr alloys, Acta Biomater. 48 (2017) 499–520.
- [17] R.-G. Guan, A.F. Cipriano, Z.-Y. Zhao, J. Lock, D. Tie, T. Zhao, T. Cui, H. Liu, Development and evaluation of a magnesium-zinc-strontium alloy for biomedical applications – alloy processing, microstructure, mechanical properties, and biodegradation, Mater. Sci. Eng. C Mater. Biol. Appl. 33 (7) (2013) 3661–3669.
- [18] A.F. Cipriano, A. Sallee, R.G. Guan, Z.Y. Zhao, M. Tayoba, J. Sanchez, H.N. Liu, Investigation of magnesium-zinc-calcium alloys and bone marrow derived mesenchymal stem cell response in direct culture, Acta Biomater. 12 (2015) 298–321.
- [19] M.E. Iskandar, A. Aslani, H. Liu, The effects of nanostructured hydroxyapatite coating on the biodegradation and cytocompatibility of magnesium implants, J. Biomed. Mater. Res. Part A 101A (8) (2013) 2340–2354.
- [20] S.S.A. El-Rahman, Neuropathology of aluminum toxicity in rats (glutamate and GABA impairment), Pharmacol. Res. 47 (3) (2003) 189–194.
- [21] Z. Li, X. Gu, S. Lou, Y. Zheng, The development of binary Mg-Ca alloys for use as biodegradable materials within bone. Biomaterials 29 (10) (2008) 1329-1344.
- [22] X. Gu, X. Xie, N. Li, Y. Zheng, L. Qin, In vitro and in vivo studies on a Mg-Sr binary alloy system developed as a new kind of biodegradable metal, Acta Biomater. 8 (6) (2012) 2360–2374.
- [23] Y.C. Li, M.H. Li, W.Y. Hu, P. Hodgson, C. Wen, Biodegradable Mg-Ca and Mg-Ca-Y alloys for Regenerative Medicine, Mater. Sci. Forum (2010) 654-656. 2192-
- [24] N. Li, Y.F. Zheng, Novel magnesium alloys developed for biomedical application: a review, J. Mater. Sci. Technol. 29 (6) (2013) 489–502.
- [25] J.L. Wang, S. Mukherjee, D.R. Nisbet, N. Birbilis, X.B. Chen, In vitro evaluation of biodegradable magnesium alloys containing micro-alloying additions of strontium, with and without zinc, J. Mater. Chem. B 3 (45) (2015) 8874–8883.
- [26] Y. Li, C. Wen, D. Mushahary, R. Sravanthi, N. Harishankar, G. Pande, P. Hodgson, Mg-Zr-Sr alloys as biodegradable implant materials, Acta Biomater. 8 (8) (2012) 3177–3188.
- [27] M. Li, P. He, Y. Wu, Y. Zhang, H. Xia, Y. Zheng, Y. Han, Stimulatory effects of the degradation products from Mg-Ca-Sr alloy on the osteogenesis through regulating ERK signaling pathway, Sci. Rep. 6 (2016).
 [28] A. Scuteri, E. Donzelli, D. Foudah, C. Caldara, J. Redondo, G. D'Amico, G. Tredici,
- [28] A. Scuteri, E. Donzelli, D. Foudah, C. Caldara, J. Redondo, G. D'Amico, G. Tredici, M. Miloso, Mesengenic differentiation: comparison of human and rat bone marrow mesenchymal stem cells, Int. J. Stem Cells 7 (2) (2014) 127.
- [29] A.F. Cipriano, A. Sallee, R.-G. Guan, A. Lin, H. Liu, A Comparison study on the degradation and cytocompatibility of Mg-4Zn-x Sr Alloys in direct culture, ACS Biomater. Sci. Eng. 3 (4) (2017) 540–550.
- [30] W. Jiang, Q. Tian, T. Vuong, M. Shashaty, C. Gopez, T. Sanders, H. Liu, Comparison study on four biodegradable polymer coatings for controlling magnesium degradation and human endothelial cell adhesion and spreading, ACS Biomater. Sci. Eng. 3 (6) (2017) 936–950.

- [31] A.F. Cipriano, A. Sallee, M. Tayoba, M.C.C. Alcaraz, A. Lin, R.-G. Guan, Z.-Y. Zhao, H. Liu, Cytocompatibility and early inflammatory response of human endothelial cells in direct culture with Mg-Zn-Sr alloys, Acta Biomater. 48 (2017) 499–520.
- [32] I. Johnson, K. Akari, H. Liu, Nanostructured hydroxyapatite/poly (lactic-co-glycolic acid) composite coating for controlling magnesium degradation in simulated body fluid, Nanotechnology 24 (37) (2013) 375103.
- [33] A. Oyane, H.M. Kim, T. Furuya, T. Kokubo, T. Miyazaki, T. Nakamura, Preparation and assessment of revised simulated body fluids, J. Biomed. Mater. Res. Part A 65 (2) (2003) 188–195.
- [34] T.Y. Nguyen, C.G. Liew, H. Liu, An in vitro mechanism study on the proliferation and pluripotency of human embryonic stems cells in response to magnesium degradation, PLoS One 8 (10) (2013) e76547.
- [35] M. Aljarrah, M. Medraj, Thermodynamic modelling of the Mg–Ca, Mg–Sr, Ca–Sr and Mg–Ca–Sr systems using the modified quasichemical model, Calphad 32 (2) (2008) 240–251.
- [36] H.S. Brar, J. Wong, M.V. Manuel, Investigation of the mechanical and degradation properties of Mg-Sr and Mg-Zn-Sr alloys for use as potential biodegradable implant materials, J. Mech. Behav. Biomed. Mater. 7 (2012) 87-95.
- [37] I.S. Berglund, H.S. Brar, N. Dolgova, A.P. Acharya, B.G. Keselowsky, M. Sarntinoranont, M.V. Manuel, Synthesis and characterization of Mg-Ca-Sr alloys for biodegradable orthopedic implant applications, J. Biomed. Mater. Res. B Appl. Biomater. 100 (6) (2012) 1524–1534.
- [38] N.T. Kirkland, N. Birbilis, J. Walker, T. Woodfield, G.J. Dias, M.P. Staiger, In-vitro dissolution of magnesium–calcium binary alloys: clarifying the unique role of calcium additions in bioresorbable magnesium implant alloys, J. Biomed. Mater. Res. B Appl. Biomater. 95 (1) (2010) 91–100.
- [39] Y. Zhong, J.O. Sofo, A.A. Luo, Z.-K. Liu, Thermodynamics modeling of the Mg-Sr and Ca-Mg-Sr systems, J. Alloys Compd. 421 (1) (2006) 172-178.
- [40] N. Kirkland, N. Birbilis, M. Staiger, Assessing the corrosion of biodegradable magnesium implants: a critical review of current methodologies and their limitations, Acta Biomater. 8 (3) (2012) 925–936.
- [41] R. Willumeit, F. Feyerabend, N. Huber, Magnesium degradation as determined by artificial neural networks, Acta Biomater. 9 (10) (2013) 8722–8729.
- [42] N.A. Agha, R. Willumeit-Römer, D. Laipple, B. Luthringer, F. Feyerabend, The degradation interface of magnesium based alloys in direct contact with human primary osteoblast cells, PloS One 11 (6) (2016) e0157874.
- [43] A. Witecka, A. Yamamoto, W. Święszkowski, Influence of SaOS-2 cells on corrosion behavior of cast Mg-2.0 Zn0. 98Mn magnesium alloy, Colloids Surf., B 150 (2017) 288–296.
- [44] M.B. Kannan, A. Yamamoto, H. Khakbaz, Influence of living cells (L929) on the biodegradation of magnesium-calcium alloy, Colloids Surf., B 126 (2015) 603– 606
- [45] J. Zhang, S. Hiromoto, T. Yamazaki, J. Niu, H. Huang, G. Jia, H. Li, W. Ding, G. Yuan, Effect of macrophages on in vitro corrosion behavior of magnesium alloy, J. Biomed. Mater. Res. Part A 104 (10) (2016) 2476–2487.
- [46] I. Johnson, W. Jiang, H. Liu, The effects of serum proteins on magnesium alloy degradation in vitro, Sci. Rep. 7 (1) (2017) 14335.
- [47] R. Willumeit, J. Fischer, F. Feyerabend, N. Hort, U. Bismayer, S. Heidrich, B. Mihailova, Chemical surface alteration of biodegradable magnesium exposed to corrosion media, Acta Biomater. 7 (6) (2011) 2704–2715.

- [48] T. Kokubo, Formation of biologically active bone-like apatite on metals and polymers by a biomimetic process, Thermochim. Acta 280 (1996) 479–490.
- [49] T. Kokubo, Apatite formation on surfaces of ceramics, metals and polymers in body environment, Acta Mater. 46 (7) (1998) 2519–2527.
- [50] H. Nygren, N. Bigdeli, L. Ilver, P. Malmberg, Mg-corrosion, hydroxyapatite, and bone healing, Biointerphases 12 (2) (2017) 02C407.
- [51] V. Wagener, S. Virtanen, Protective layer formation on magnesium in cell culture medium, Mater. Sci. Eng., C 63 (2016) 341–351.
- [52] J.-W. Park, K.-B. Park, J.-Y. Suh, Effects of calcium ion incorporation on bone healing of Ti6Al4V alloy implants in rabbit tibiae, Biomaterials 28 (22) (2007) 3306–3313
- [53] S.N. Nayab, F.H. Jones, I. Olsen, Effects of calcium ion implantation on human bone cell interaction with titanium, Biomaterials 26 (23) (2005) 4717–4727.
- [54] M.J. Berridge, P. Lipp, M.D. Bootman, The versatility and universality of calcium signalling, Nat. Rev. Mol. Cell Biol. 1 (1) (2000) 11–21.
- [55] K. Zhang, J. Chen, The regulation of integrin function by divalent cations, Cell Adhes. Migration 6 (1) (2012) 20–29.
- [56] B. Leitinger, A. McDowall, P. Stanley, N. Hogg, The regulation of integrin function by Ca 2+, Biochimica et Biophysica Acta (BBA)-Molecular, Cell Res. 1498 (2) (2000) 91–98.
- [57] J.P. Xiong, T. Stehle, S. Goodman, M. Arnaout, Integrins, cations and ligands: making the connection, J. Thromb. Haemost. 1 (7) (2003) 1642–1654.
- [58] L. Moore, I. Pastan, ENERGY-DEPENDENT CALCIUM UPTAKE BY FIBROBLAST MICROSOMES, Ann. N. Y. Acad. Sci. 307 (1) (1978) 177–194.
- [59] T. Afroze, G. Yang, A. Khoshbin, M. Tanwir, T. Tabish, A. Momen, M. Husain, Calcium efflux activity of plasma membrane Ca2+ ATPase-4 (PMCA4) mediates cell cycle progression in vascular smooth muscle cells, J. Biol. Chem. 289 (10) (2014) 7221–7231.
- [60] J. Whitfield, A. Boynton, J. MacManus, M. Sikorska, B. Tsang, The regulation of cell proliferation by calcium and cyclic AMP, Molecular and cellular biochemistry 27 (3) (1979) 155–179.
- [61] M. Brini, T. Calì, D. Ottolini, E. Carafoli, The plasma membrane calcium pump in health and disease, FEBS J. 280 (21) (2013) 5385–5397.
- [62] L. Lipskaia, A.M. Lompré, Alteration in temporal kinetics of Ca2+ signaling and control of growth and proliferation, Biol. Cell 96 (1) (2004) 55–68.
- [63] M. Tada, T. Yamamoto, Y. Tonomura, Molecular mechanism of active calcium transport by sarcoplasmic reticulum, Physiol. Rev. 58 (1) (1978) 1–79.
- [64] Q. Tian, M. Deo, L. Rivera-Castaneda, H. Liu, Cytocompatibility of magnesium alloys with human urothelial cells: a comparison of three culture methodologies, ACS Biomater. Sci. Eng. 2 (9) (2016) 1559–1571.
- [65] E. Gentleman, Y.C. Fredholm, G. Jell, N. Lotfibakhshaiesh, M.D. O'Donnell, R.G. Hill, M.M. Stevens, The effects of strontium-substituted bioactive glasses on osteoblasts and osteoclasts in vitro, Biomaterials 31 (14) (2010) 3949–3956.
- [66] E.S. Place, L. Rojo, E. Gentleman, J.P. Sardinha, M.M. Stevens, Strontium-and zinc-alginate hydrogels for bone tissue engineering, Tissue Eng. Part A 17 (21– 22) (2011) 2713–2722.
- [67] R. Kroes, E. Den Tonkelaar, A. Minderhoud, G. Speijers, D. Vonk-Visser, J. Berkvens, G. Van Esch, Short-term toxicity of strontium chloride in rats, Toxicology 7 (1) (1977) 11–21.
- [68] A.F. Cipriano, T. Zhao, I. Johnson, R.-G. Guan, S. Garcia, H. Liu, In vitro degradation of four magnesium-zinc-strontium alloys and their cytocompatibility with human embryonic stem cells, J. Mater. Sci. Mater. Med. 24 (4) (2013) 989–1003.